Synthesis, characterization, optical, thermogravimetric and single crystal x-ray diffraction studies of 3-aminocoumarin based κ^3-*N,O,O*-tridentate/ κ^2-*N,O*-bidentate Schiff base transition metal complexes

Abstract

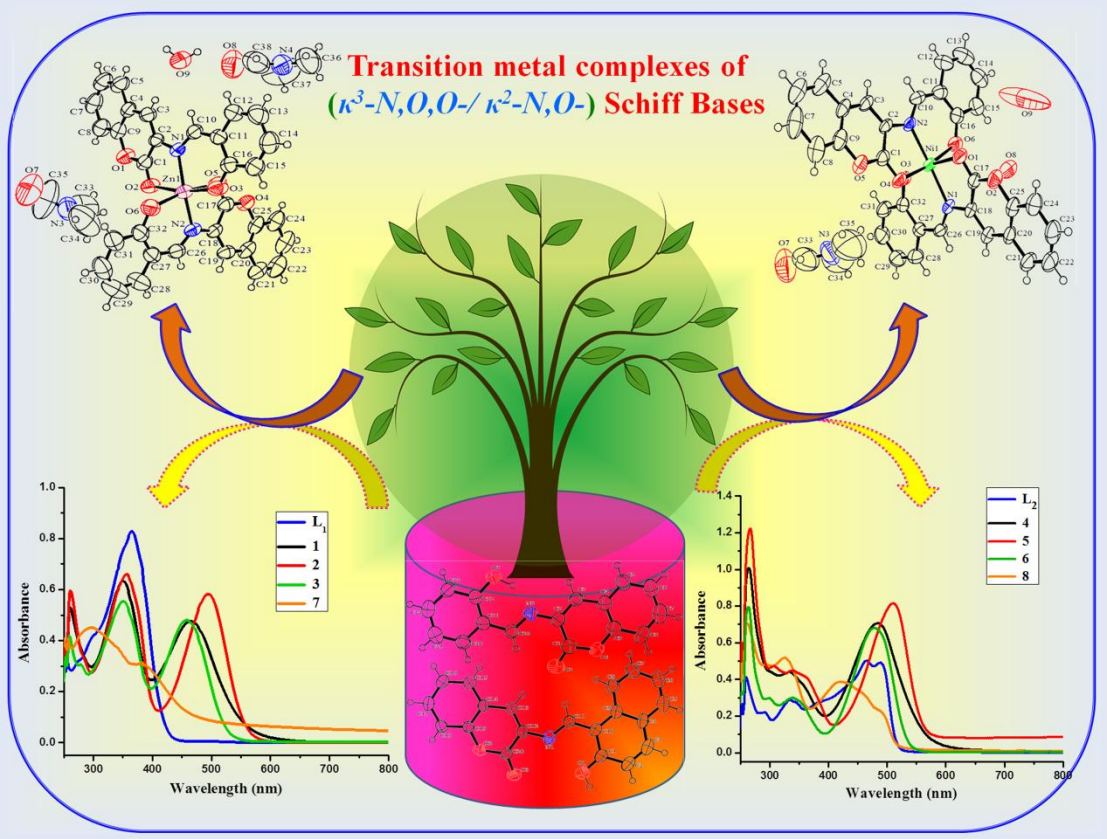

3-Amino coumarin based Schiff base ligands 3-(2-hydroxyphenylmethylidene amino) coumarin (**HL^1**) and 3-(2-hydroxy-1-naphthylmethylidene amino) coumarin (**HL^2**) were synthesized by usual acid catalyzed condensation methods. The reaction of **HL^1** or **HL^2** and metal acetates in 2:1 molar ratios in refluxing toluene affords access to a new series of neutral mononuclear transition metal complexes [M^{II}-κ^3-bis-*N,O,O*-tridentate Schiff base-L^1/ L^2] {L^1; M^{II} = Co (**1**), Ni (**2**) or Zn (**3**); L^2; M^{II} = Co (**4**), Ni (**5**) or Zn (**6**)} and [M^{II}-κ^2-bis-*N,O*-bidentate Schiff base-L^1/ L^2] {L^1; M^{II} = Cu (7); L^2; M^{II} = Cu (8)}. **L^1-L^2** and **1-8**. These compounds were thoroughly characterized by MALDI-TOF-MS, IR, ^{1}H and ^{13}C NMR, UV-visible, fluorescence spectroscopic methods, CV, TGA/DTA methods. The unambiguous crystal structure for **L^1**, **L^2**, complexes **2** and **3** were

determined by means of single crystal X-ray diffraction technique. The IR, UV-visible, EPR spectral studies along with magnetic susceptibly measurements clearly suggest the κ^3-*N,O,O*-tridentate- coordination mode of L^1 and L^2 towards cobalt(II), nickel(II) and zinc(II) metal ions in **1-6** while κ^2-*N,O*-bidentate-coordination mode towards copper(II) metal ions in **7** and **8**. All of the newly synthesized compounds feature a direct band gap semiconducting nature and exhibit band gap energy in the range of 1.7-2.23 eV. The thermograms of $\mathbf{L^1}$ and $\mathbf{L^2}$ clearly give a sharp endothermic peak on DTA curves at 187.5 and 220.3 ºC respectively, without any significant mass loss on DTG curves, due to the phase change that can be assigned to the melting points of these compounds whereas for their complexes **1-8**, decomposition starts before their melting points. Compared to the cyclic voltammogram of $\mathbf{L^1}$ and $\mathbf{L^2}$, their complexes **1-3** and **6-8** did not display any additional peak, in the cathodic or anodic scan under the similar experimental conditions which suggests that these complexes are primarily electro active with respect to the ligand fragment wherein the redox active transition metal cations are apparently present in silent mode.

5.1. Introduction

Schiff base ligands with active and well-defined frameworks are considered as 'privileged ligands' because they are easily prepared by condensation of aldehydes or ketones with amines and are able to stabilize different metals in various oxidation states [1]. These compounds are some of the most widely used organic compounds. They are used as pigments and dyes, catalysts, intermediates in organic synthesis, and as polymer stabilisers. *N, O*-Schiff bases have also been shown to exhibit a broad range of biological activities, including antifungal, antibacterial, antimalarial, antiproliferative, anti-inflammatory, antiviral, [2] and antipyretic properties. Their complexes are extensively studied due to synthetic flexibility, selectivity and sensitivity towards variety of metal ions [3]. The coordination geometry of these complexes depends upon the electronic configuration and size of the metal ions, repulsions between non-bonded atoms in different ligand arms, and the inherent rigidity due to the presence of aromatic rings. Schiff bases are important systems in asymmetric catalysis [4] and their transition metal complexes can often mimic biological sites; they are therefore of great interest as enzyme

models. [5-14] Their five- and six-coordinated complexes can display a variety of structural and magnetic properties. Transition and non-transition metals complexes with Schiff base ligands are appeared to display promising applications as optoelectronic materials due to their outstanding photo and electroluminescent properties, and the ease of synthesis that readily allows structural modification for optimization of material properties [15]. A number of transition and inner transition metal complexes with bi-, tri- and tetradentate Schiff bases containing nitrogen and oxygen donor atoms have been shown to play important role in biological systems and represent interesting models for metalloenzymes, which efficiently catalyze the reduction of dinitrogen and dioxygen [16]. Biological studies of Cu(II) coordination compounds with Schiff bases of polyamines with heterocyclic aldehydes as ligands have been reported [17,18]. Purposefully, authors have selected polyamines and heterocyclic aldehydes (2-thiophene-carboxaldehyde and 2-furaldehyde) because of its coordinative, conformational and physicochemical properties as well as to mimic biological systems and mechanisms in the process of drug design. In view of aforesaid importance of Schiff bases and their complexes and relatively few reports on complexes with an *N,O,O*-tridentate Schiff base-containing coordination environment yielding octahedral geometry, we have synthesized, we herein present a facile synthesis a novel Schiff base ligands 3-[(2-hydroxyarylmethylideneamino)coumarin {aryl = phenyl (**L**^{1}) or naphthyl (**L**^{2})} and their mononuclear transition metal complexes of cobalt(II), nickel(II), copper(II) and zinc(II) in which L^{1} and L^{2} evidently display κ^{3}-*N,O,O*-tridentate- coordination mode towards cobalt(II), nickel(II) and zinc(II) metal ions whereas these ligands evidently display κ^{2}-*N,O*-bidentate-coordination mode towards copper(II) metal ion.

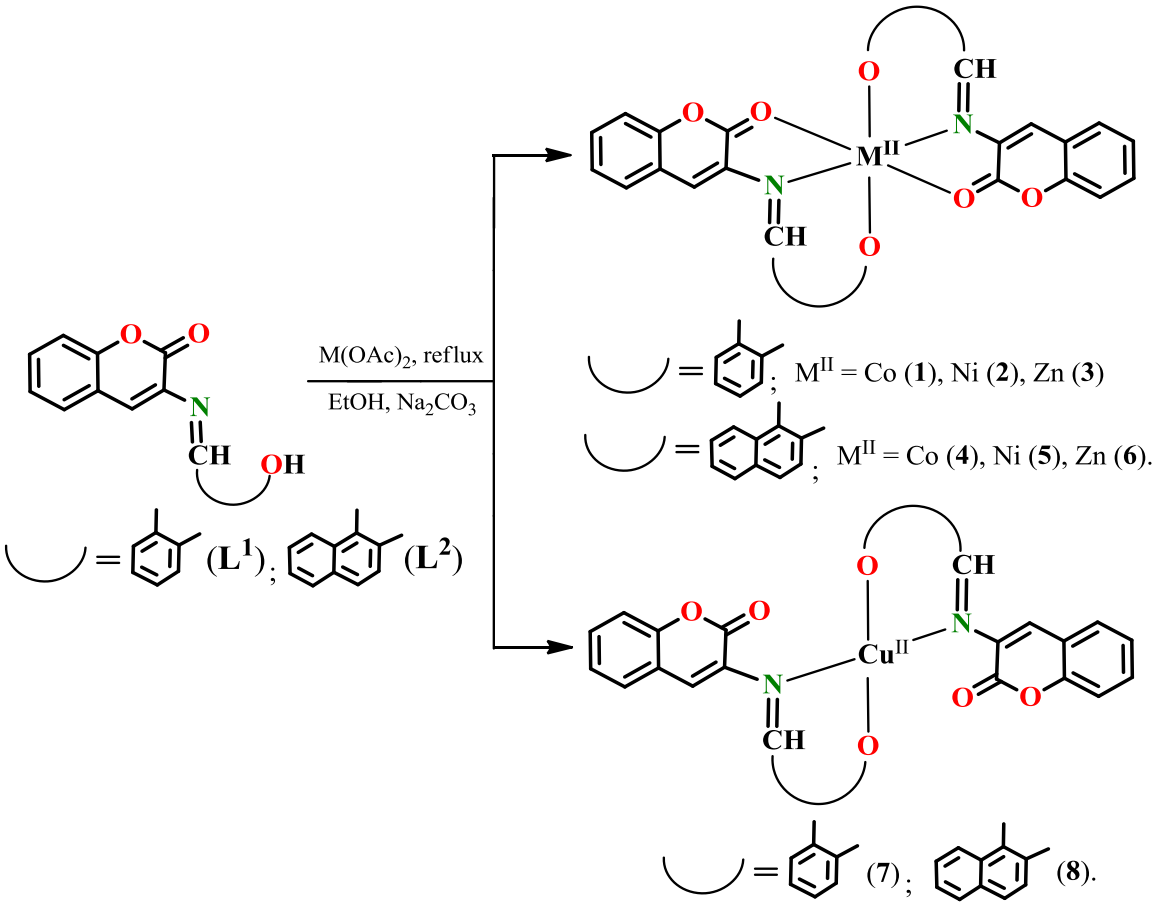

Scheme 1: Synthesis of κ^3-*N*,*O*,*O*-tridentate Schiff base and κ^2-*N*,*O*-bidentate Schiff base transition metal complexes **1-8**.

5.2. Result and Discussion

5.2.1. Synthesis and characterization

3-Amino coumarin based Schiff base ligands 3-(2-hydroxyphenylmethylidene amino) coumarin (**HL^1**) and 3-(2-hydroxy-1-naphthylmethylidene amino) coumarin (**HL^2**) were synthesized by usual acid catalyzed condensation methods reported elsewhere [19]. Reaction of **HL^1** or **HL^2** and metal acetates in 2:1 molar ratios in refluxing toluene affords access to a new series of neutral mononuclear transition metal complexes [M^{II}-κ^3-bis-*N*,*O*,*O*-tridentate Schiff base-L^1/ L^2] {L^1; M^{II} = Co (**1**), Ni (**2**) or Zn (**3**); L^2; M^{II} = Co (**4**), Ni (**5**) or Zn (**6**)} and [M^{II}-κ^2-bis-*N*,*O*-bidentate Schiff base-L^1/ L^2] {L^1; M^{II} = Cu (7); L^2; M^{II} = Cu (8)}. **L^1-L^2** and **1-8** exhibit moderate solubility of common organic

solvents however these are fairly soluble in DMSO or DMF. These compounds are stable in the solution and in solid state over a period of days. Newly synthesized compounds were characterized by microanalysis, and relevant spectroscopic techniques such as ES-MS, IR, NMR, UV-visible absorption and emission spectroscopies. These were further characterized by magnetic moment and TGA/DTA analysis. Elemental analysis and spectroscopic data mutually suggest the formation of the desired structures. The unambiguous molecular structures of **L^1**, **L^2**, **2** and **3** were determined by means of single crystal X-ray diffraction study.

5.2.2. IR spectral study

Selected IR data of the Schiff base-**L^1** and Schiff base-**L^2** and their complexes **1-8** are given in experimental section. The IR spectra of the complexes are compared with those of corresponding free ligands **L^1** and **L^2** in order to determine the co-ordination sites that may be involved in chelation. The IR spectra of the free ligands showed a strong band in the region 1615cm^{-1} which is characteristic of the azomethine group [20]. The IR band arises due to the azomethine group υ(C=N) for the complexes **1-8** showed a modest shift of 3-12 cm^{-1}towards lower frequency, compared to its position in corresponding free ligand L^1/L^2. This indicates the co-ordination of the azomethine nitrogen [21] in all the complexes **1-8**. Further, disappearance of υ(O-H) band from the IR spectra of all the complexes indicating the subsequent deprotonation of the phenolic proton prior to co-ordination in **1-8** . Remarkably, a careful comparison of IR spectra of L^1 and L^2 with their corresponding complexes **1-8** clearly suggests that lactone ring carbonyl of these ligands, display selectivity in coordination with various metals ions. For instance, the υ(C=O) stretching frequency for **1-6** showed a modest shift of 27-61 cm^{-1} towards lower frequency (Fig. 1), compared to its position in corresponding free ligand L^1/L^2. This indicates the co-ordination of the lactone ring carbonyl with Co^{II}, Ni^{II} and Zn^{II} complexes **1-6**. However, this band does not show any significant change in the Cu^{II} complexes **7** and **8**, compared to corresponding free ligands. This highlights the non-involvement of lactone ring carbonyl in the coordination with

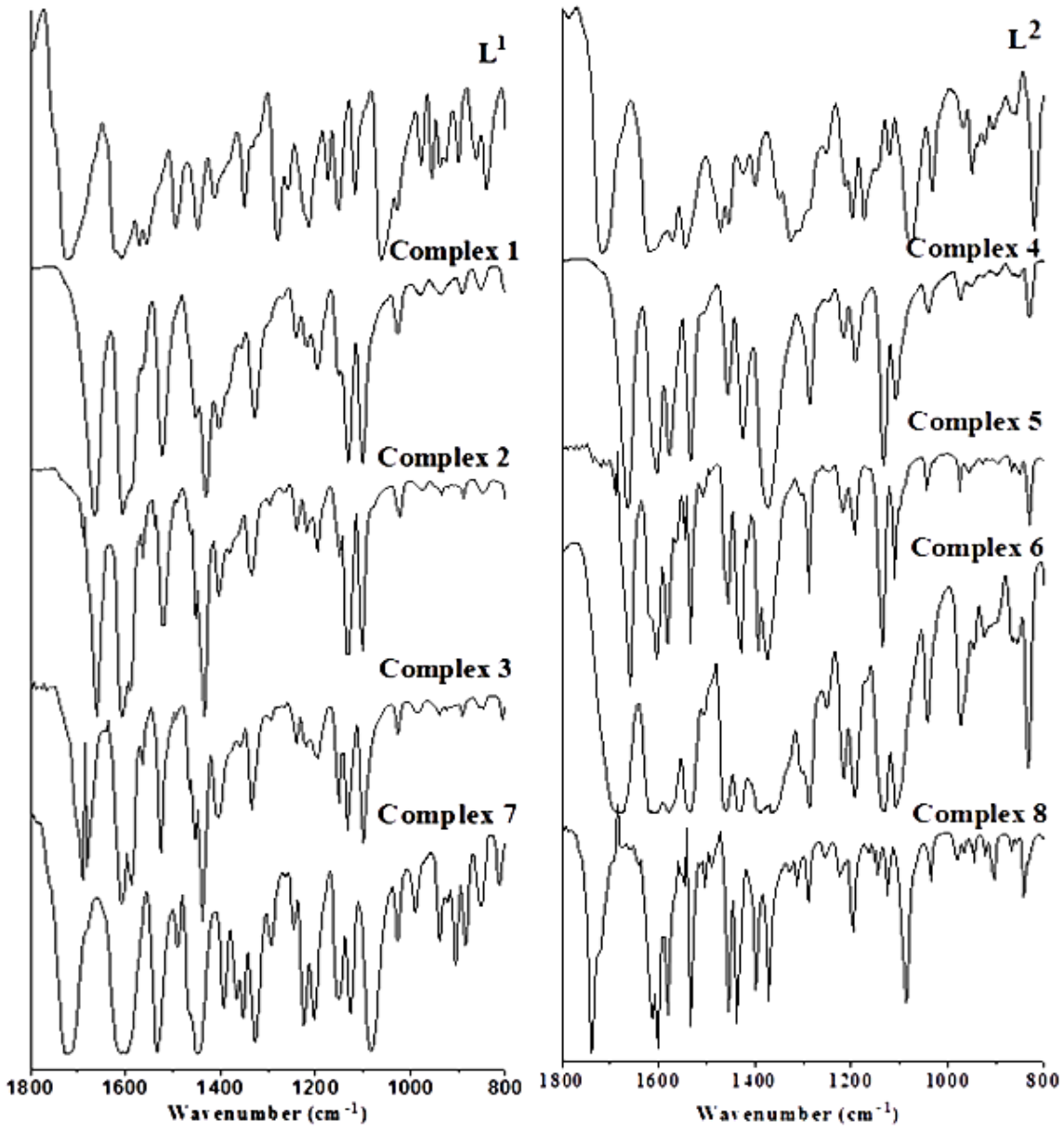

Fig. 1. Merged IR spectra of L^1/ L^2 and their respective κ^3-*N,O,O*-tridentate/ κ^2-*N,O*-bidentate Schiff base transition metal complexes **1-8**.

copper(II) centre which is further supported by EPR spectral studies, discussed latter. Thus, IR spectral study reveals the κ^3-*N,O,O*-tridentate coordination mode of L^1 and L^2 towards Co^{II}, Ni^{II} and Zn^{II} metal ions in complexes **1-6** and κ^2-*N,O*-bidentate coordination mode of L^1 and L^2 towards Cu^{II} metal ions in complexes **7-8**. The bands appeared at ~1200 cm^{-1} and 1000 cm^{-1} for were ascribed to the six membered lactone (C-O) and the phenolic C-O stretching vibrations respectively. The lactone C-O band are shifted downfield in the case of all the metals Co(II), Ni(II), Cu(II), Zn(II) for both the

ligands. This is also supported by the disappearance of the υ(OH) band in the range 3410-3424 cm^{-1}.

5.2.3. NMR spectral study

A comparison of ^{1}H NMR spectral data of **3** and **6** with the ^{1}H NMR spectra of corresponding free Schiff base ligands $\mathbf{L^1}$ and $\mathbf{L^2}$ further supplements the conclusion drawn from IR data. The ^{1}H NMR spectra of L^1 and L^2 display signals due to imine proton (-**H**C=N) at 9.486 and 10.196 ppm, and phenolic O-**H** proton at 12.983 ppm and 15.188 ppm, respectively. As expected [22], the characteristic ^{1}H signals due to imine (-**H**C=N) protons of **3** and **6** experience significant up-field shift, compared to its position in the free ligand. Moreover, the disappearance of OH signals from the ^{1}H NMR spectra of **3** and **6** indicates deprotonation of the hydroxyl group of L^1/ L^2 due to Zn-O bond formation. L^1 and L^2 were also characterized by ^{13}C NMR spectra and the characteristic NMR data are summarized in the experimental section.

5.2.4. Single Crystal X-ray diffraction study

Suitable single crystals for crystallographic study were grown from slow evaporation of acetone (for $\mathbf{L^1}$, $\mathbf{L^2}$) and dimethylformamide (for **2** and **3**) solutions. $\mathbf{L^1}$ and $\mathbf{L^2}$ crystallize in monoclinic $P2_1/n$ and orthorhombic $Pna2_1$ space groups and their X-ray crystal structures show asymmetric unit contains full molecule of [$C_{16}H_{11}NO_3$] and [$C_{20}H_{13}NO_3$], respectively. Whereas both of the nickel(II) **2** and zinc(II) **3** complexes crystallize as **2**.DMSO.$2H_2O$ and **3.**2DMSO.H_2O in triclinic P -1 space groups. The X-ray crystal structures of **2** and **3** shows one complete molecule in their asymmetric units. There are four such units of $\mathbf{L^1}$ and $\mathbf{L^2}$ and two such units of **2** and **3** in their respective unit cells. The *ORTEP* view at 50 % probability with atom numbering scheme for $\mathbf{L^1}$, $\mathbf{L^2}$, **2** and **3** is shown in Fig. 2a-d. Selected bond angles (º) and bond lengths (Å) for $\mathbf{L^1}$, $\mathbf{L^2}$, **2** and **3** are tabulated in Table 1 whereas details about data collection, refinement, and structure solution are provided in Table 2.

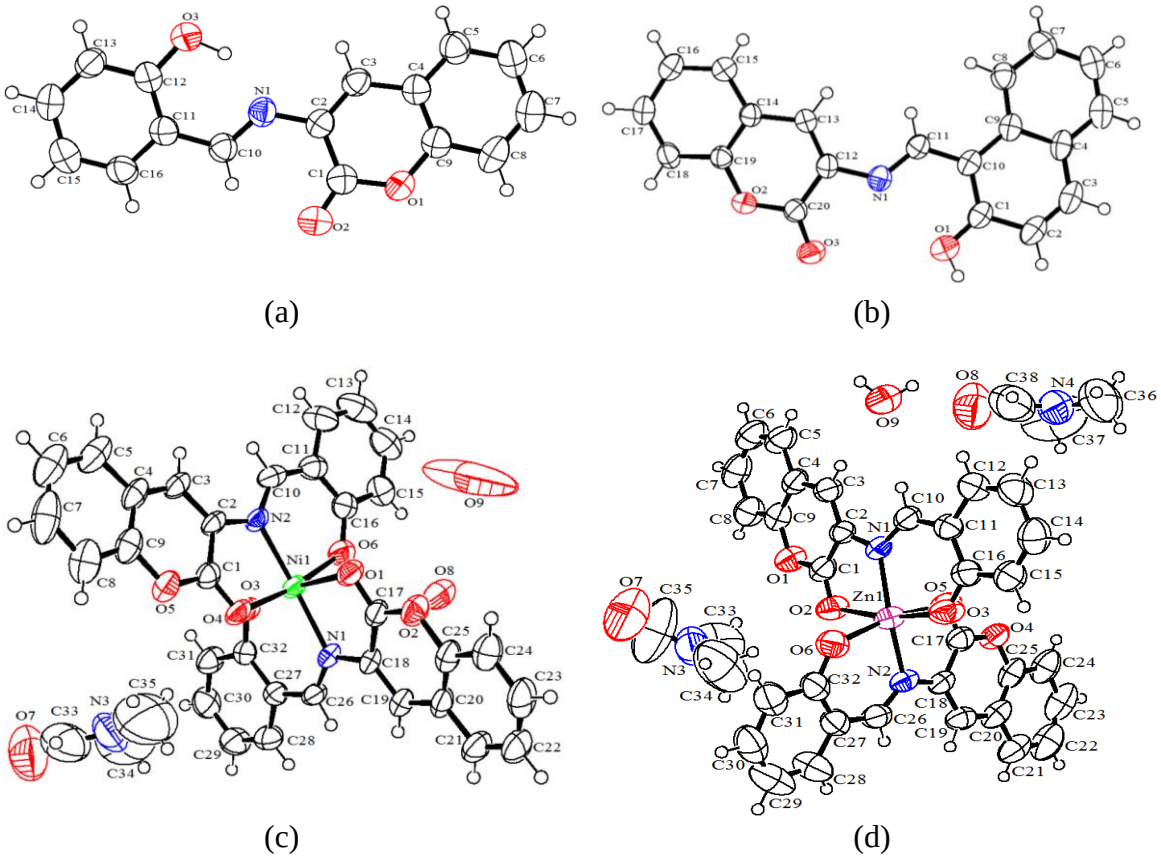

Fig. 2. The ORTEP view at 50% probability for (a) $\mathbf{L^1}$, (b) $\mathbf{L^2}$, (c) **2** and (d) **3** with atom numbering scheme

Notably, the ketonic and phenolic groups are present in the opposite direction in the free lagand L^1, probably to minimize the electronic repulsions. However, these groups of L^1 have flipped along the same orientation involving a free rotation of coumarin moiety across C2-N1 bond in its nickel(II) **2** and zinc(II) **3** complexes. This is indeed necessary for L^1 to exhibit κ^3-*N,O,O*- tridentate mode of bonding towards these metal ions to form an octahedral complexes. However, these groups in L^2 are already present in the desired orientation to exhibit κ^3-*N,O,O*-tridentate coordination mode towards cobalt(II), nickel(II) and zinc(II) metal ions in their respective complexes **4-6**, probably due to presence of bulkier 2-hydroxy-1-naphthylmethylidene group. In the complexes **2** and **3**, each nickel(II) or zinc(II) centers are bonded with the available coordination sites of Schiff base $\mathbf{L^1}$ through two imine nitrogen, two phenolic oxygen atoms and two lactone carbonyl oxygen atoms wherein $\mathbf{L^1}$ exhibits κ^3-*N,O,O*-tridenatate mode of coordination.

The angles between the two O−M−N planes deviates from coplanarity and O−M−O, and N−M−N angles differ significantly from 90° in both the complexes **2** and **3**. The geometry around the metal ions in **2-3** is thus essentially distorted octahedral. It appears that M–O and M–N bond lengths (involving phenolic oxygen atoms and imine nitrogen atoms) around nickel(II) center in **2** are comparable with the similar distances around the zinc center in **3** whereas M–O bond lengths (involve oxygen atoms of lactone ring carbonyls) around nickel(II) center in **2** are significantly shorter than the similar distances around the zinc(II) center in **3**. The participation of lactone ring carbonyl group in the coordination with metal ions in **2** and **3** is reflected by an appreciable increase in the corresponding C-O bond lengths from 1.20 Å in $\mathbf{L^1}$ to 1.21-1.23 Å. Further, the involvement of the imine (CH=N) group of L^1 in complexation is supported by an appreciable decrease in the C=N bond length from 1.405(5) Å (for $\mathbf{L^1}$) to ~ 1.28 Å (for **2-3**). These observations are consistent with results of IR spectral study. The bond lengths (Å) of the donor atoms to the central metal atom along with the other structural parameters (Table zz) for these complexes **2** and **3** are found in the normal range and in a good agreement with those observed for the similar group containing compounds. [19,23-25].

Table 1. Selected bond angles (°) and bond lengths (Å) of the crystal structures **L[1]**, **L[2]**, **2** and **3**

Bond length (Å)							
L[1]		**L[2]**		**2**. DMSO.2H_2O		**3.** 2DMSO.H_2O	
O(1)-C(9)	1.382(5)	O(2)-C(19)	1.375(4)	Ni(1)-O(1)	2.151(3)	Zn(1)-O(3)	1.977(4)
O(1)-C(1)	1.377(5)	O(2)-C(20)	1.366(4)	Ni(1)-O(3)	1.981(3)	Zn(1)-O(6)	1.988(4)
O(3)-C(12)	1.348(5)	O(3)-C(20)	1.202(4)	Ni(1)-O(4)	2.170(4)	Zn(1)-O(5)	2.362(4)
N(1)-C(2)	1.405(5)	N(1)-C(12)	1.406(4)	Ni(1)-O(6)	2.001(4)	Zn(1)-O(2)	2.290(4)
N(1)-C(10)	1.295(5)	N(1)-C(11)	1.310(4)	Ni(1)-N(1)	2.022(4)	Zn(1)-N(1)	2.053(4)
O(2)-C(1)	1.200(5)	O(1)-C(1)	1.281(5)	Ni(1)-N(2)	2.020(4)	Zn(1)-N(2)	2.078(5)
C(11)-C(12)	1.380(6)	C(1)-C(10)	1.431(5)	O(3)-C(32)	1.284(6)	O(1)-C(9)	1.387(7)
C(11)-C(10)	1.456(6)	C(6)-C(5)	1.354(6)	O(6)-C(16)	1.300(6)	O(1)-C(1)	1.368(7)
C(2)-C(1)	1.475(6)	C(14)-C(13)	1.447(4)	N(1)-C(18)	1.418(6)	N(1)-C(10)	1.294(7)
C(4)-C(9)	1.384(6)	C(14)-C(15)	1.394(5)	N(1)-C(26)	1.280(6)	N(1)-C(2)	1.417(7)
C(4)-C(3)	1.431(5)	C(3)-C(4)	1.428(6)	N(2)-C(2)	1.397(6)	O(7)-C(35)	1.14(3)
C(4)-C(5)	1.387(6)	C(4)-C(5)	1.407(6)	N(2)-C(10)	1.282(7)	O(8)-C(38)	1.180(14)
C(9)-C(8)	1.396(6)	C(10)-C(11)	1.409(4)	O(4)-C(1)	1.230(6)	O(2)-C(1)	1.208(7)
				O(1)- C(17)	1.229(6)	O(5)-C(17)	1.215(7)
Bond Angles (deg)							
C(1)-O(1)-C(9)	122.5(4)	C(20)-O(2)-C(19)	122.6(3)	O(1)-Ni(1)-O(4)	87.11(14)	O(3)-Zn(1)-O(6)	102.0(2)
C(10)-N(1)-C(2)	124.8(4)	C(11)-N(1)-C(12)	125.7(3)	O(3)-Ni(1)-O(1)	171.09(13)	O(3)-Zn(1)-O(5)	89.55(19)
C(10)-C(11)-C(12)	122.2(4)	C(14)-C(19)-O(2)	121.2(3)	O(3)-Ni(1)-O(4)	88.78(15)	O(3)-Zn(1)-O(2)	166.58(16)
C(16)-C(11)-C(12)	119.0(4)	C(18)-C(19)-O(2)	116.5(3)	O(3)-Ni(1)-O(6)	96.48(16)	O(3)-Zn(1)-N(1)	91.95(18)
C(16)-C(11)-C(10)	118.7(4)	C(18)-C(19)-C(14)	122.3(3)	O(3)-Ni(1)-N(1)	92.46(15)	O(3)-Zn(1)-N(2)	101.52(18)
C(3)-C(2)-N(1)	118.3(4)	C(13)-C(12)-N(1)	127.5(3)	O(3)-Ni(1)-N(2)	95.33(15)	O(6)-Zn(1)-O(5)	163.78(17)
C(1)-C(2)-N(1)	122.2(4)	C(20)-C(12)-N(1)	110.9(3)	O(6)-Ni(1)-O(1)	88.80(15)	O(6)-Zn(1)-O(2)	87.57(18)
C(1)-C(2)-C(3)	119.5(4)	O(1)-C(1)-C(2)	119.4(3)	O(6)-Ni(1)-O(4)	169.94(14)	O(6)-Zn(1)-N(1)	106.56(19)
C(13)-C(12)-O(3)	117.7(4)	C(10)-C(1)-O(1)	122.6(3)	O(6)-Ni(1)-N(1)	98.52(16)	O(6)-Zn(1)-N(2)	91.48(19)
C(11)-C(10)-N(1)	119.8(4)	O(3)-C(20)-O(2)	118.0(3)	O(6)-Ni(1)-N(2)	91.57(16)	O(2)-Zn(1)-O(5)	83.17(16)
O(2)-C(1)-O(1)	115.5(4)	C(12)-C(20)-O(2)	116.5(3)	N(1)-Ni(1)-O(1)	79.63(14)	N(1)-Zn(1)-O(5)	84.15(17)
C(2)-C(1)-O(1)	116.9(4)	C(12)-C(20)-O(3)	125.5(3)	N(1)-Ni(1)-O(4)	89.78(14)	N(1)-Zn(1)-O(2)	76.14(17)
C(8)-C(9)-O(1)	116.5(4)	C(10)-C(11)-N(1)	121.6(3)	N(2)-Ni(1)-O(1)	91.68(14)	N(1)-Zn(1)-N(2)	154.82(19)
C(4)-C(9)-O(1)	121.1(4)			N(2)-Ni(1)-O(4)	79.38(14)	N(2)-Zn(1)-O(5)	74.88(17)
				N(2)-Ni(1)-N(1)	166.48(15)	N(2)-Zn(1)-O(2)	87.50(16)

Table 2 Crystal data and structure refinement for compounds **L^1**, **L^2**, **2** and **3**

Identification code	**L^1**	**L^2**	**2**. DMSO.$2H_2O$	**3.** 2DMSO.H_2O
Empirical formula	$C_{16}H_{11}NO_3$	$C_{20}H_{13}NO_3$	$C_{35}H_{27}N_3O_9Ni$	$C_{38}H_{36}N_4O_9Zn$
Formula weight	265.27	315.33	692.29	758.13
Temperature (K)	293.0	293.0	293.0	293.0
Wavelength (Å)	1.5418	1.5418	0.71073	1.5418
Crystal system	Monoclinic	Orthorhombic	Triclinic	Triclinic
space group	$P2_1/n$	$Pna2_1$	P -1	P -1
Unit cell dimensions(Å/ °)	a = 14.272(2) b = 6.4691(5) c = 14.692(2) α/°= 90 β/°=111.934(16) γ/°= 90	a = 23.4634(10) b = 4.7465(3) c =13.1081(7) α/°= 90 β/°= 90 γ/°= 90	a = 9.4694(7) b = 14.1566(11) c = 15.3147(9) α/°= 65.130(7) β/°= 85.961(5) γ/°= 73.080(7)	a = 9.3646(8) b = 14.330(2) c = 15.279(2) α/°= 66.484(14) β/°= 86.787(9) γ/°= 73.020(11)
Volume/$Å^3$	1258.3(3)	1459.83(14)	1778.8(2)	1793.8(4)
Z	4	4	2	2
Calculated density/Mg/m^3	1.4002	1.4346	1.304	1.4035
Absorption coefficient/ m/mm^{-1}	0.804	0.792	0.600	1.467
F(000)	553.9	656.0	716.0	104.0
Crystal size/mm^3	0.6 × 0.09 × 0.06 mm	0.5 × 0.1 × 0.05 mm	0.3 × 0.12 × 0.05 mm	0.3 × 0.1 × 0.04 mm
Theta range for data collection	10.92 to 144.8°	7.54 to 143.88°	6.22 to 58.34°	9.9 to 144.22 deg.
Limiting indices	$-17 \le h \le 16$, $-7 \le k \le 5$, $-18 \le l \le 17$	$-28 \le h \le 28$, $-5 \le k \le 3$, $-15 \le l \le 14$	$-12 \le h \le 12$, $-17 \le k \le 16$, $-19 \le l \le 18$	$-4 \le h \le 11$, $-17 \le k \le 17$, $-18 \le l \le 18$
Reflections collected / unique	7393/ 2444 [R (int) = 0.0974]	2699/1768 [R(int)=0.0146]	14389/ 9598 [R(int) = 0.0415]	10168/6752 [R(int)=0.0511]
Completeness to theta = 24.99				99.9 %
Data / restraints / parameters	2444/0/184	1768/0/216	7929/0/435	6752/0/476
Goodness-of-fit on F^2	0.993	1.071	0.914	1.028
Final R indices [I>2sigma(I)]	R_1 = 0.0800, wR_2 = 0.1531	R_1 = 0.0498, wR_2 = 0.1239	R_1 = 0.0830, wR_2 = 0.2505	R_1 = 0.0846, wR_2 = 0.1885
Largest diff. peak and hole/ e $Å^{-3}$	0.38/-0.38	0.27/-0.26	1.16/-0.56	0.65/-0.60

5.2.5. UV-visible spectral and magnetic moment study

The recognition of Schiff bases-L^1 and L^2 and their metal complexes **1-8** were investigated by UV-visible spectroscopy in DMSO solution. These spectral studies were carried out in a freshly prepared solution in DMSO at room temperature. The UV-visible absorption spectra of the **L^1**, **L^2** and mononuclear complexes **1-8** are shown in Fig. 3 and Fig. 4. The ligand L^1 displays a single prominent absorption band at 364 nm which may be assigned to $\pi \rightarrow \pi^*$ (phenyl) transitions while L^2 display absorption bands at 260, 334, 465 and 489 nm, respectively.

All the complexes **1-8** exhibit maximum absorbance at ~350, ~260, 349, 264, 265, 341, 298 and 261 nm with the molar extinction coefficient values of 63298, 59284, 55585, 100008, 121310, 300027, 44948 and 71063, respectively. The bands appeared in the range of 325-380 nm these complexes may be attributed to the intraligand charge transfer transitions associated with imine (-C=N) moieties. In general, the differential electronic spectra of **1-8** clearly suggest alterations in structural features of the molecular framework. The shorter absorption band may be assigned to π→π* (phenyl) transitions and the longer absorption band may be assigned to n→π* transitions whereas the absorption bands as shown in Table 3. The ligand to metal charge transfer transition bands in these complexes appeared at 400-510 nm regions. Expectedly, the copper(II) complexes **7** and **8** display a broad band at 755 and 728 nm, respectively, similar to those reported for copper(II) ions in square planar environment [26]. The magnetic moment data along with the UV-visible spectral data (Table xx) is consistent with an octahedral environment [27, 28] around cobalt(II), nickel(II) and zinc(II) ions in their respective complexes **1-6** while the data suggest square planar environment around copper(II) ions in the complexes **7-8**.

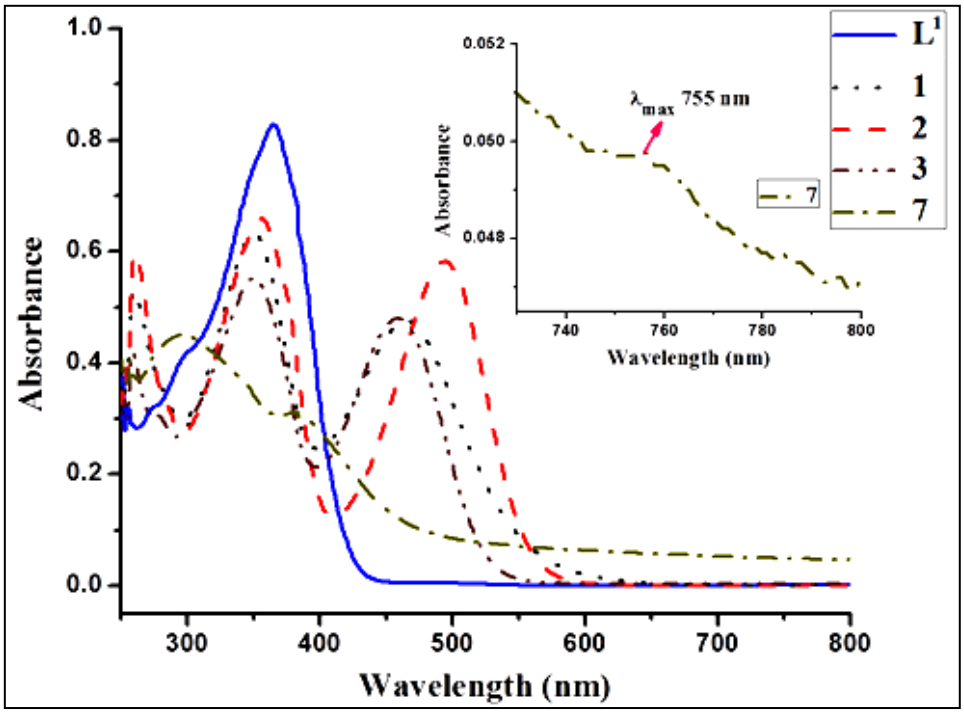

Fig. 3. UV-visible absorption spectra of L^1 and its metal complexes at room temperature in 10^{-5} M DMSO solution.

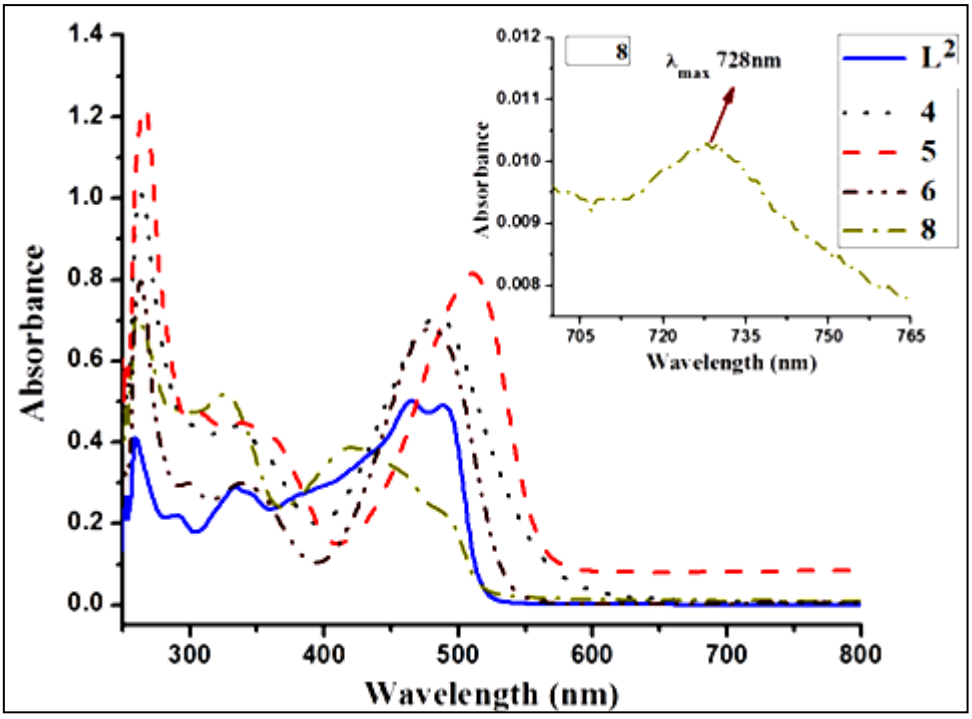

Fig. 4. UV-visible absorption spectra of L^2 and its metal complexes at room temperature in 10^{-5} M DMSO solution

Table 3 UV-visible, magnetic moment data, fluorescence and optical band gaps for L^1, L^2 and their metal complexes 1-8.

Entry	λ_{max} nm (ε L Mol^{-1} cm^{-1})	Magnetic Moment (μ_{eff} BM)	Fluorescence spectral data		Optical Band gap (eV)
			λ_{ex} nm	λ_{em} (nm) (Intensity)	
L^1	364(83169) n→π*	-	364	438(107.4) π*→ n 601(78.1)	2.179
L^2	260(41683) π→π* 334(28973) π→π* 465(50315) n→π* 489(48771)	-	260 334	326(89.6) π*→ π 354(104.3) π*→ n 375(36.1) 411(56.2)	2.2064
1	260(53033) π →π* 350(63298) $^4T_{1g}(F)\rightarrow{}^4T_{1g}(P)$ 465(47872) $^4T_{1g}(F)\rightarrow{}^4A_{2g}$ 718(823) $^4T_{1g}(F)\rightarrow{}^4T_{2g}$	3.9	350 465	414(77.4) $^4T_{1g}(P)\rightarrow{}^4T_{1g}(F)$ 436(70.6) 540(4.1) $^4A_{2g}\rightarrow{}^4T_{1g}(F)$	1.7315
2	260(59284) π →π* 356(6680) $^3A_{2g}\rightarrow{}^3T_{1g}(P)$ 494(58166) $^3A_{2g}\rightarrow{}^3T_{1g}(F)$ 666(476) $^3A_{2g}\rightarrow{}^3T_{2g}$	2.9	356 494	389 $^3T_{1g}(P)\rightarrow{}^3A_{2g}$ 581(2.5) $^3T_{1g}(F)\rightarrow{}^3A_{2g}$	2.235
3	260(41994) 349(55585) MLCT 459(48285)	dia	349 459	441(389.1) 550 (54.0) 620(133.2)	2.0415

4	264(100008) π →π*	4.3	264	329(107.7) π*→ π	1.569
	333(44732)			354(109.2)	
	$^4T_{1g}(F)\rightarrow{}^4T_{1g}(P)$		333	379(53.7)	
	485(71063) $^4T_{1g}(F)\rightarrow{}^4A_{2g}$			412(105.3) $^4T_{1g}(P)\rightarrow{}^4T_{1g}(F)$	
	771(543) $^4T_{1g}(F)\rightarrow{}^4T_{2g}$				
5	265(121310) π →π*	3.22	306	362(93.5) π*→ π	1.7864
	306(47226)			402(104.5)	
	339(44732) $^3A_{2g}\rightarrow{}^3T_{1g}(P)$		339	413(79.3)	
	510(81754) $^3A_{2g}\rightarrow{}^3T_{1g}(F)$				
	692(8185) $^3A_{2g}\rightarrow{}^3T_{2g}$				
6	263(79220)	dia	263	328(126.8)	2.01
	341(300027) MLCT			353(123.4)	
	480(68014)			385(52.8)	
			341	413(98.2)	
7	298(44948) π→π*	1.9	298	398	2.086
	380(30640) $^2B_{1g}\rightarrow{}^2E_g$		380	519(9.9) π*→ n	
	668(5608) $^2B_{1g}\rightarrow{}^2A_{1g}$				
	755(4979)				
8	261(71063) π→π*	2.1	261	329(66.3) π*→ π	1.9211
	325(51780) $^2B_{1g}\rightarrow{}^2E_g$			356(82.2) π*→ n	
	418(38634) $^2B_{1g}\rightarrow{}^2A_{1g}$		325	367(49.9)	
	728(1051)			407(55.4)	

5.2.6. Fluorescence spectral study

The fluorescence properties of the free ligands L^1, L^2 and their metal complexes **1-8** were studied at room temperature (298 K) in the DMSO solution. The fluorescence spectra of these compounds are shown in Fig. 5 and Fig. 6 and the related data is summarized in Table 4. L^1 gave two emission bands at 438 nm, 601 nm upon excitation at 364 nm and in the similar way its complex **1** gave two emission bands at 414 nm and at 436 upon excitation at a single wavelength of 350 nm. Additionally, **1** gave another emission band at 540 nm upon excitation at 465 nm. Distinctly, complex **2** gave only single emission band at 389 nm and at 581 nm upon excitation at 356 and 494 nm, respectively. Complex **3** fluoresces at 441 nm upon excitation at 349 nm as well as at 550 nm and 620 nm upon excitation at 459 nm. On the other hand, L^2 fluoresces two emissions bands at 326, 354 and 375, 411 nm upon excitation at 260 and 334 nm, respectively. Similarly, its cobalt(II) complex **4** gave two emission bands 329, 354 nm and 379, 412 nm upon excitation at 264 nm and 333 nm, respectively. Whereas nickel(II) complex **5** displays two bands at 362, 402 nm upon excitation at 306 nm, however when excited at 339 nm, it gave a single emission band at 413 nm. Distinctly, its zinc(II) complex **6** display three bands at 328, 353 and 385 nm when excited at 263 nm and a single band at 413 nm upon excitation at 341 nm. Moreover, copper(II) complexes **7** and **8** display differential fluorescence emission properties

which can be clearly seen in Table 4. Literature reports suggest that the fluorescence properties of any compound largely depends upon the molecular arrangements, achieved by means of polymorphism, conformational rigidity of the fluorophore (dihedral angles), intermolecular interactions such as π…π or C-H…π interactions and upon the nature of substituents which can largely affect the photoinduced electron transfer processes. [29] The fluorescence emission spectra of these complexes shows a clear cut bathochromic shifts and confirm the formation of respective metal complexes **1-8**.

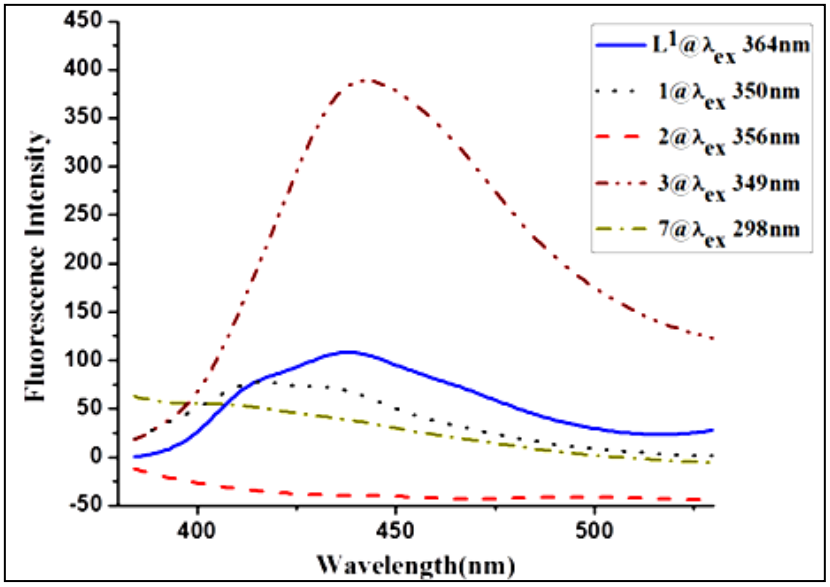

(a)

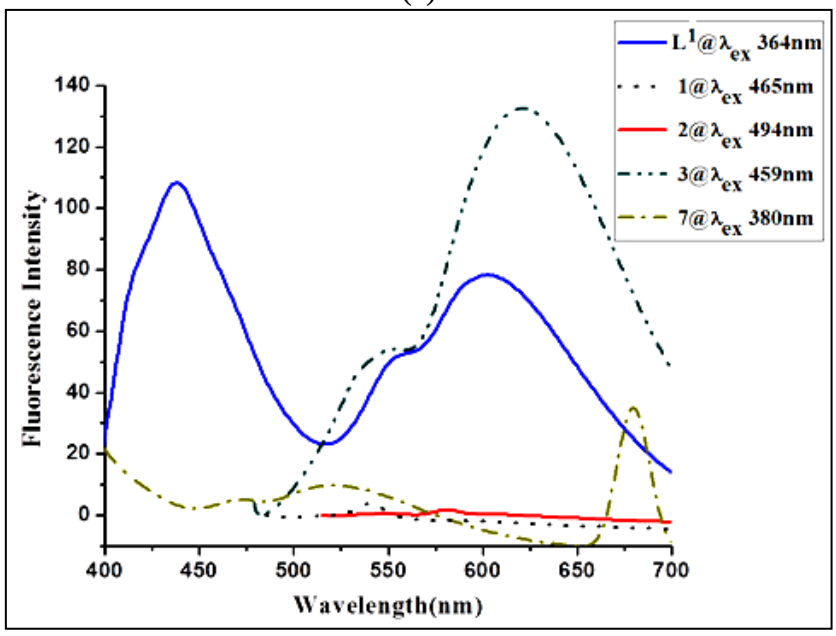

(b)

Fig. 5. Fluorescence spectra of the ligand L^1 and its metal complexes **1-3** and **7** at room temperature in 10^{-5} M DMSO solution (a) excited at lower wavelengths (b) excited at higher wavelengths

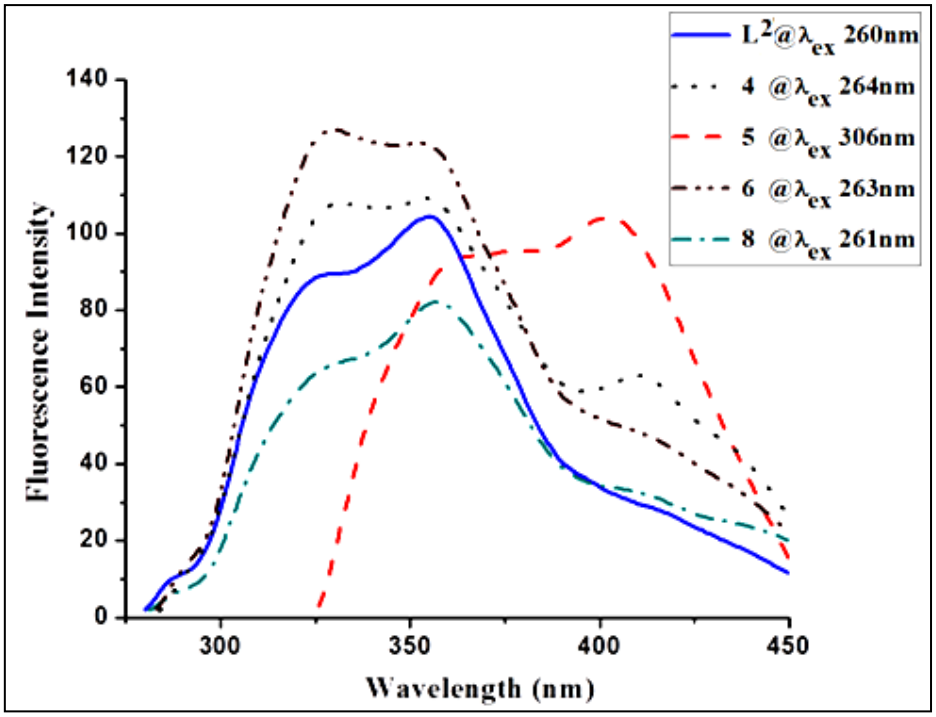

(a)

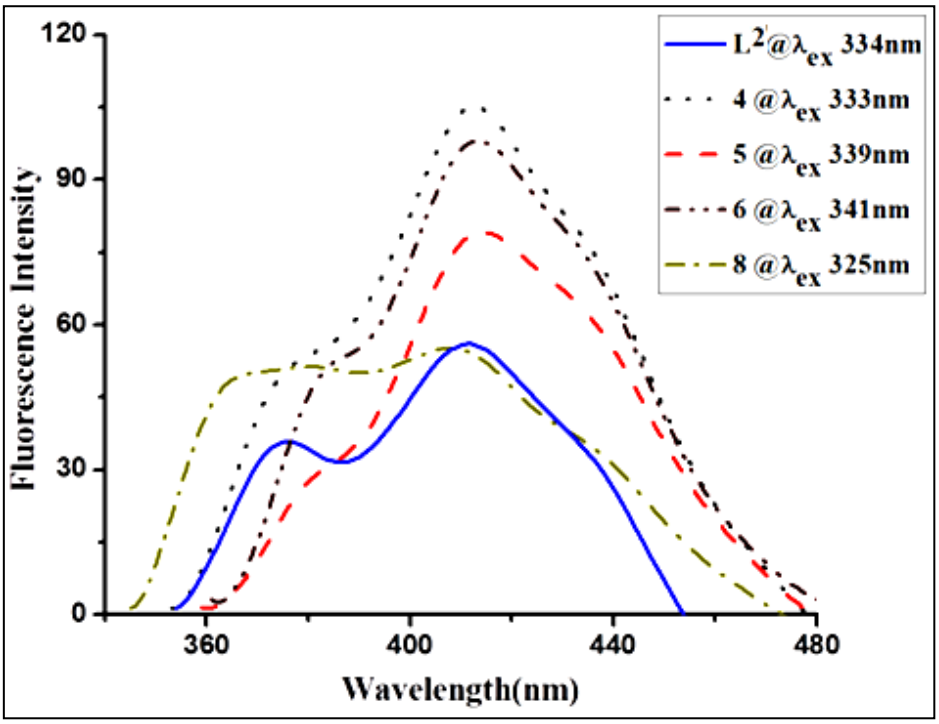

(b)

Fig. 6. Fluorescence spectra of the ligand L^2 and its metal complexes **4-6** and **8** at room temperature in 10^{-5} M DMSO solution (a) excited at lower wavelengths (b) excited at higher wavelengths.

5.2.7. ESR spectral study

The ESR spectra of copper(II) complexes (Fig. 7, 8) were recorded at 298 K in the polycrystalline state in the X- band region, using 9.1 GHZ field modulation and the g factors were quoted relative to the standard marker DPPH (g = 2.0023). Under the influence of magnetic field, epr spectrum of copper(II) complex **7**, shows one intense absorption in the high field and is isotropic due to tumbling of the molecule. Such an isotropic spectrum consisting of a broad signal giving only one g value, reportedly arises from extensive exchange coupling through misalignment of the local molecular axes between different molecules in the unit cell and enhanced spin lattice relaxation. The correlation between the g values for the complex **8** are $g\|$ (2.1753) > $g\perp$ (2.0976) >2.0023, indicating that the unpaired electron in the ground state of Cu(II) is predominantly in dx^2-y^2. The value of exchange interaction term G is estimated (geometric parameter G = 1.815 for complex **8**) from the equation [30]: G = $g\|$ – 2.0023/ $g\perp$ – 2.0023. Reports suggest that if G is less than 4.0, a significant exchange coupling is present and misalignment is appreciable. The observed value for the exchange interaction term G suggests that the complex has distorted square planar geometry.

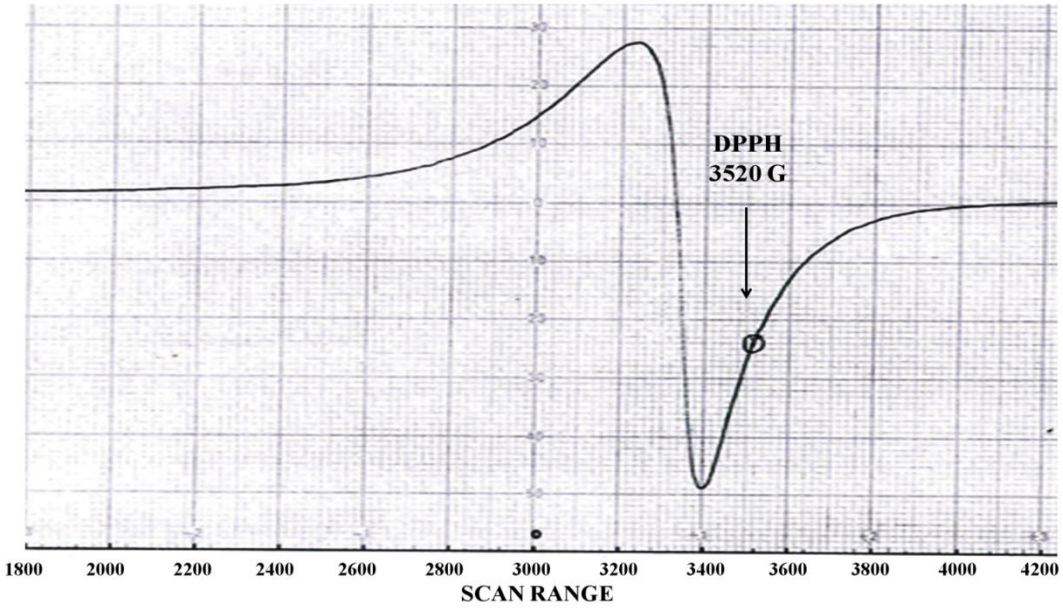

Fig. 7. ESR spectra of the complex **7** at room temperature in solid state

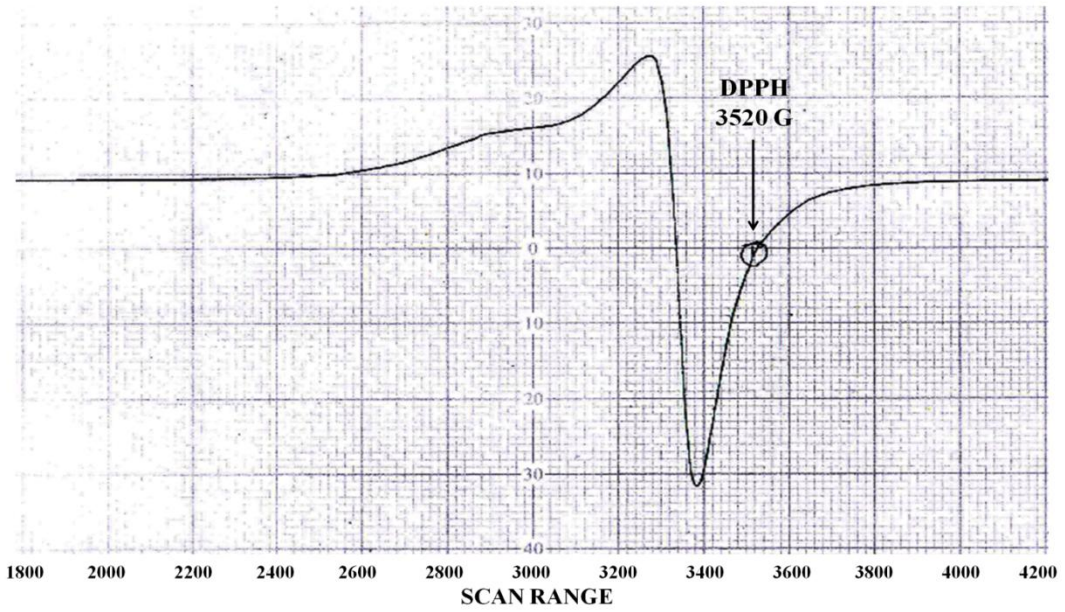

Fig. 8. ESR spectra of the complex **8** at room temperature in solid state

5.2.8. Optical band gap measurement

UV-visible spectral study performed on Schiff bases $\mathbf{L^1}$-$\mathbf{L^2}$ and their transition metal complexes **1-8** evidences the ability of these compounds to absorb in the visible regions which is indeed a primary requisite for a compound to act as a photo sensitizer for wide band-gap semiconductors (*vide supra*). This has encouraged us to investigate these compounds for their optical behavior towards wide band-gap semiconductors using UV-vis transmittance measurements.

The photon absorption corresponding to electronic excitation from the valence band to conduction band gives the optical energy band gap and its nature. By using a well known Davis and Mott equation, [31] $\alpha h\nu = [D(h\nu - Eg)]^{\gamma}$ where, constant D is the edge width parameter, a correlation between the absorption coefficient α and the incident photon energy (hν) can be established. A direct allowed transition gives the value of γ = ½ whereas direct forbidden, indirect allowed and indirect forbidden transitions give value of γ = 3/2, 2 and 3, resoectively. In order to determine optical band gap of $\mathbf{L^1}$-$\mathbf{L^2}$ and **1-8**, we applied the models for both direct and indirect transitions. Analysis of the plots obtained from $(\alpha h\nu)^2$ (direct transition) versus hν and $(\alpha h\nu)^{1/2}$ (indirect transitions) versus hν, reveal that the absorptions in these samples corresponds to direct energy gap. Extrapolating the linear part of the Tauc plot [32,33] *i. e.* a plot between $(\alpha h\nu)^{1/\gamma}$ and $h\nu$ (with γ = ½; direct allowed transition) (Fig. 9) gives a direct band gap and the calculated band gap energy (*Ea*) falls in the range of

1.7-2.23 eV (Table 3) which features a direct band gap semiconducting nature of these compounds.

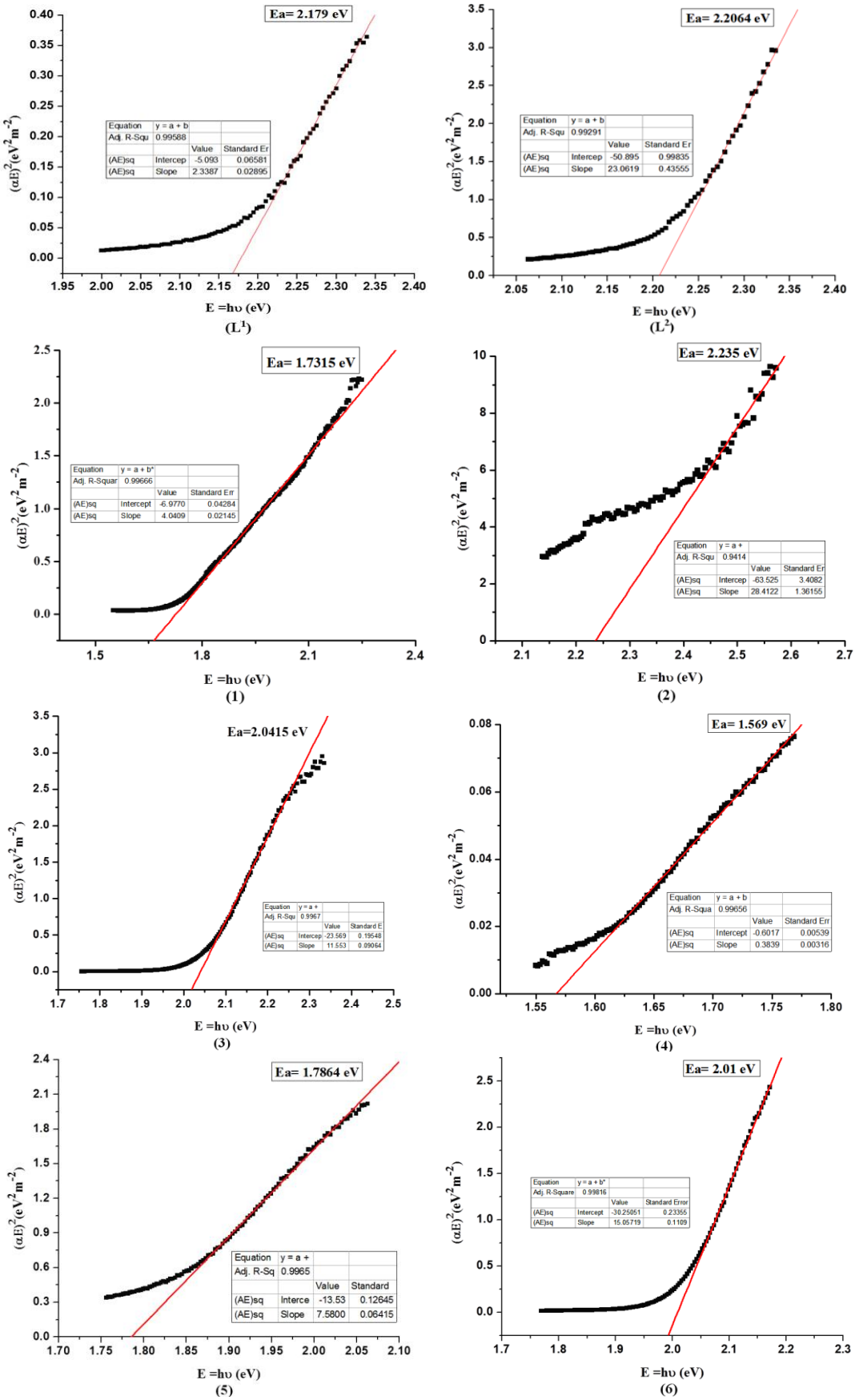

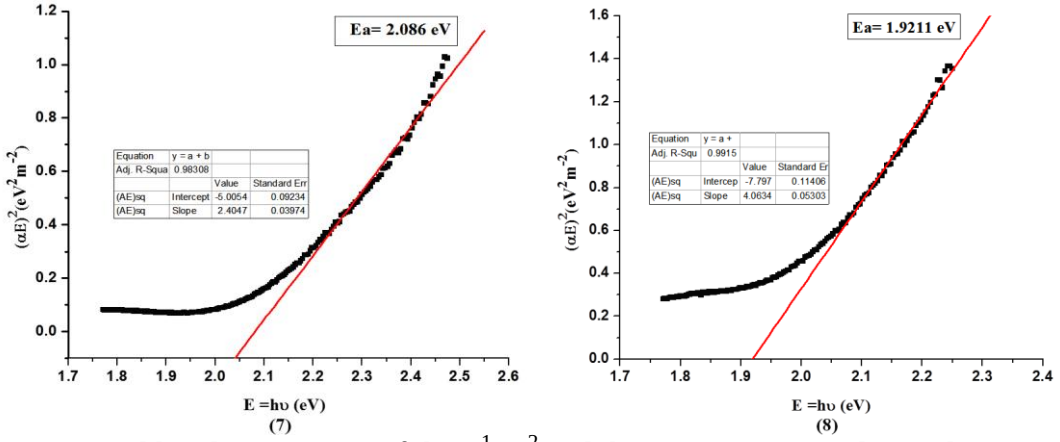

Fig. 9. Optical band gap spectra of the L^1, L^2 and their transition metal complexes **1-8**

5.2.9. MALDI-TOF MS

Matrix-assisted laser desorption/ionization time-of-flight mass spectroscopy (MALDI-TOF MS) is a relatively novel technique wherein molecule is irradiated by a nanosecond laser pulse. The system utilizes a 20 Hz pulsed nitrogen laser emitting at 337 nm [34]. The analysis of MALDI-TOF MS of the complex **1** in the positive ion mode suggest the formation of $[M+H]^+$ molecular ion, ions of single alkali metal adducts $[M+Na]^+$ and $[M+K]^+$ at m/z 588.06, 610.05 and 626.02, respectively. Nickel(II) complex **2** shows $[M+H]^+$, $[M+3]^+$, $[M-2]^+$ and $[M-31]^+$ ions at m/z 587.16, 589.16, 584.15 and 555.2 while zinc(II) complex **3** shows the fragmentation peaks at m/z 584.06, 585.06,593.06, 623.02 and 630.02 which corresponds to $[M-10+H]^+$, $[M-9+H]^+$, $[M]^+$, $[M+2H]^+$, $[M+29+H]^+$and $[M+36+H]^+$, respectively. Similar to fragmentation pattern of complex **1**, complex **5** exhibits m/z at 687.10, 709.08 and 725.05 which corresponds to $[M+H]^+$, $[M+Na]^+$ and $[M+K]^+$ molecular ions, respectively. Additionally, it shows the formation of $[M+2H+K]^+$ ion at m/z 727.05. In the case of complex **6,** the formation of various fragmentation ions such as $[M-K+H]^+$, $[M]^+$, $[M+2H]^+$, $[M+Na]^+$, $[M-H+K]^+$ and $[M+K+H]^+$ ions can be clearly visualized by the appearance of corresponding ion peaks at m/z 655.13,693.09,695.09,715.07, 731.05 and 733.04, respectively in its mass spectrum. Complexes **7** and **8** exhibit routine fragmentation peaks at the m/z 503.04, 580.07, 648.12, 650.11 and 648.01,672.06,682.02, 688.03, 692, 694, 704.01, 721.96, and these peaks evidently correspond to $[M-89+H]^+$, $[M-12+H]^+$, $[M+56+H]^+$, $[M+58+H]^+$ and $[M-44+H]^+$, $[M-20+H]^+$, $[M-4+H]^+$, $[M+H]^+$, $[M+3H]^+$, $[M+12+H]^+$, $[M+29+K]^+$, $[M+2H+K]^+$ molecular ions, respectively. The compound **8** shows the

fragmentation ions at m/z respectively. The intensity of $[M+H]^+$ ion peak was highest in case of the complexes 1, 2, 5 and second highest in the case of 8 whereas complexes 3, 6 and 7 displayed the highest intensity peaks which corresponds to $[M-10+H]^+$, $[M-H+K]^+$ and $[M+56+H]^+$, respectively. The mass spectra of these complexes are summarized below in Fig. 10.

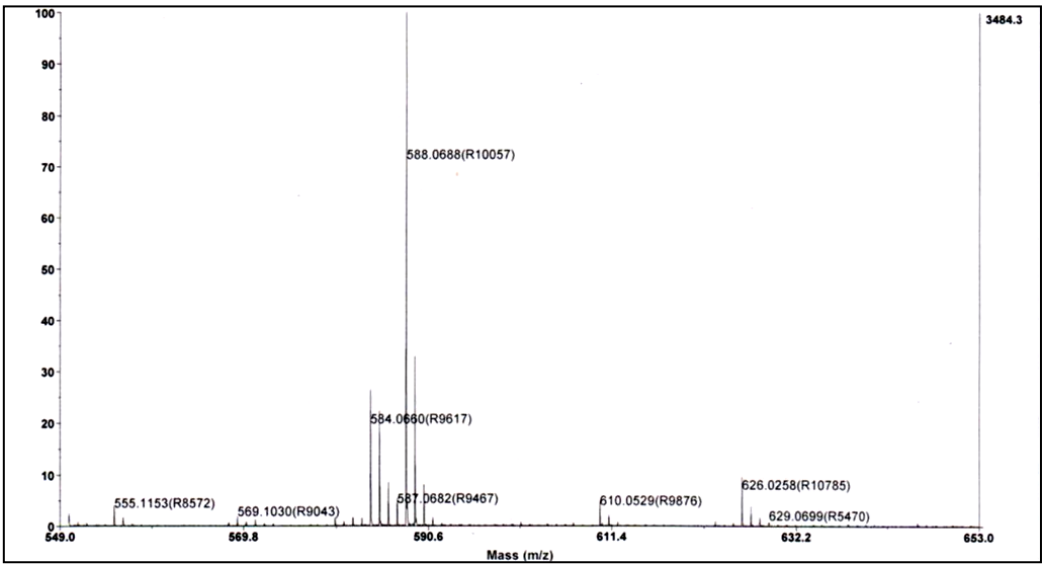

(a)

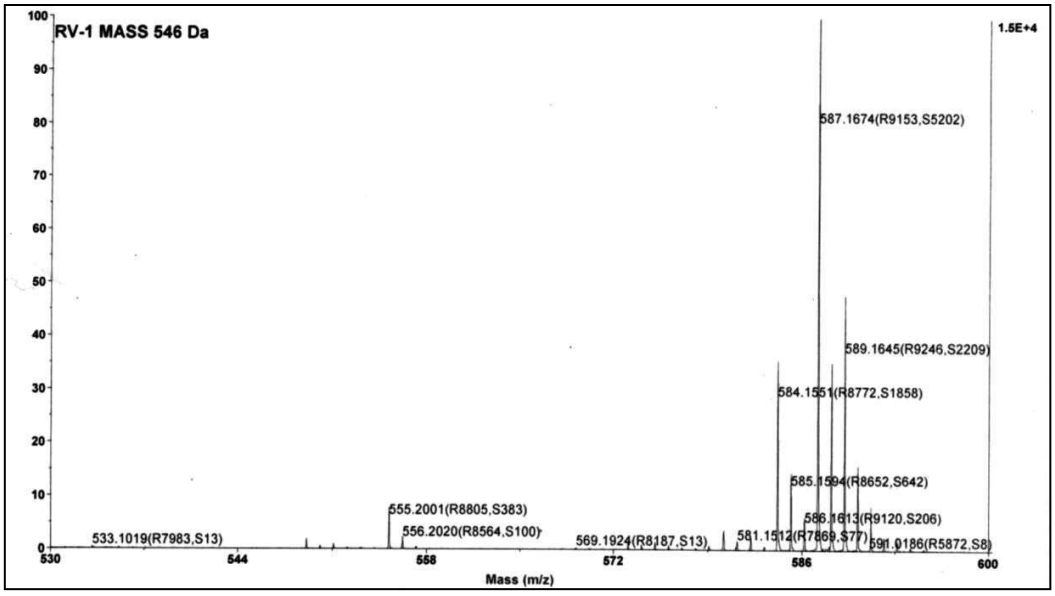

(b)

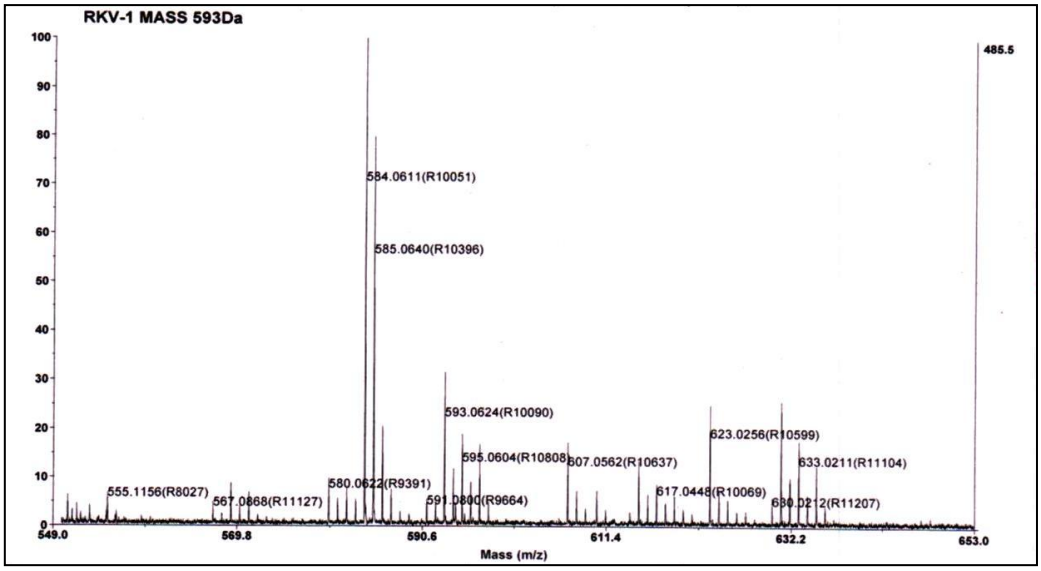
RKV-1 MASS 593Da
485.5
584.0611(R10051)
585.0640(R10396)
593.0624(R10090)
623.0256(R10599)
595.0604(R10808)
607.0562(R10637)
633.0211(R11104)
555.1156(R8027)
580.0622(R9391)
567.0868(R11127)
591.0800(R9664)
617.0448(R10069)
630.0212(R11207)
549.0
569.8
590.6
611.4
632.2
653.0
Mass (m/z)

(c)

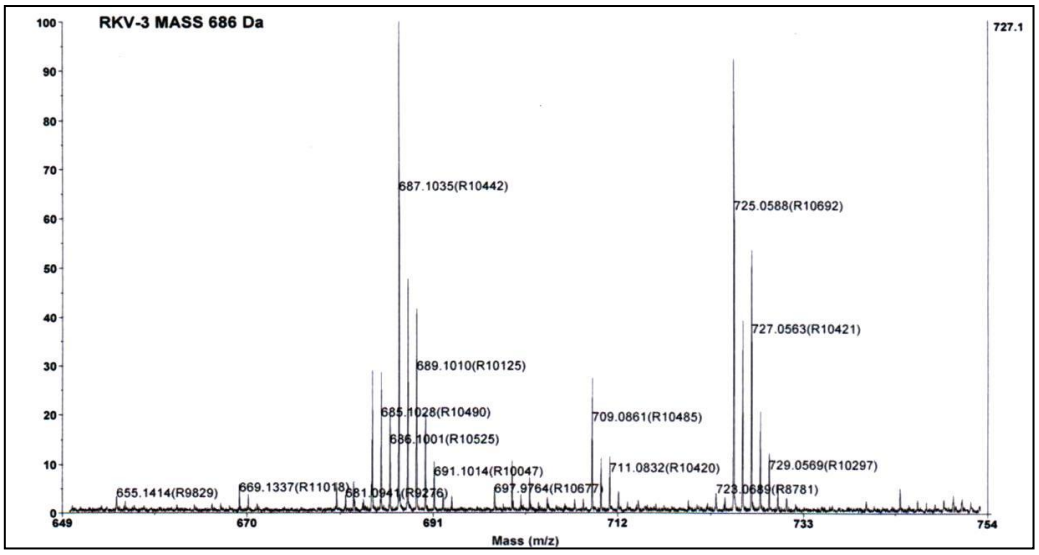
RKV-3 MASS 686 Da
727.1
687.1035(R10442)
725.0588(R10692)
727.0563(R10421)
689.1010(R10125)
685.1028(R10490)
709.0861(R10485)
686.1001(R10525)
691.1014(R10047)
711.0832(R10420)
729.0569(R10297)
655.1414(R9829)
669.1337(R11018)
697.9764(R10677)
723.0689(R8781)
649
670
691
712
733
754
Mass (m/z)

(d)

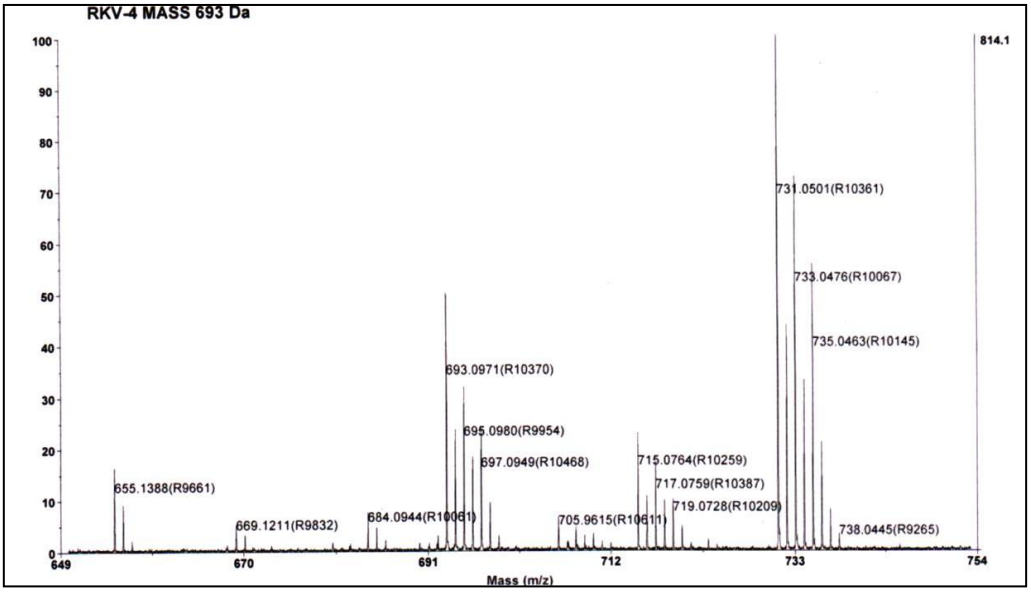
RKV-4 MASS 693 Da
814.1
731.0501(R10361)
733.0476(R10067)
735.0463(R10145)
693.0971(R10370)
695.0980(R9954)
697.0949(R10468)
715.0764(R10259)
655.1388(R9661)
717.0759(R10387)
719.0728(R10209)
669.1211(R9832)
684.0944(R10061)
705.9615(R10611)
738.0445(R9265)
649
670
691
712
733
754
Mass (m/z)

(e)

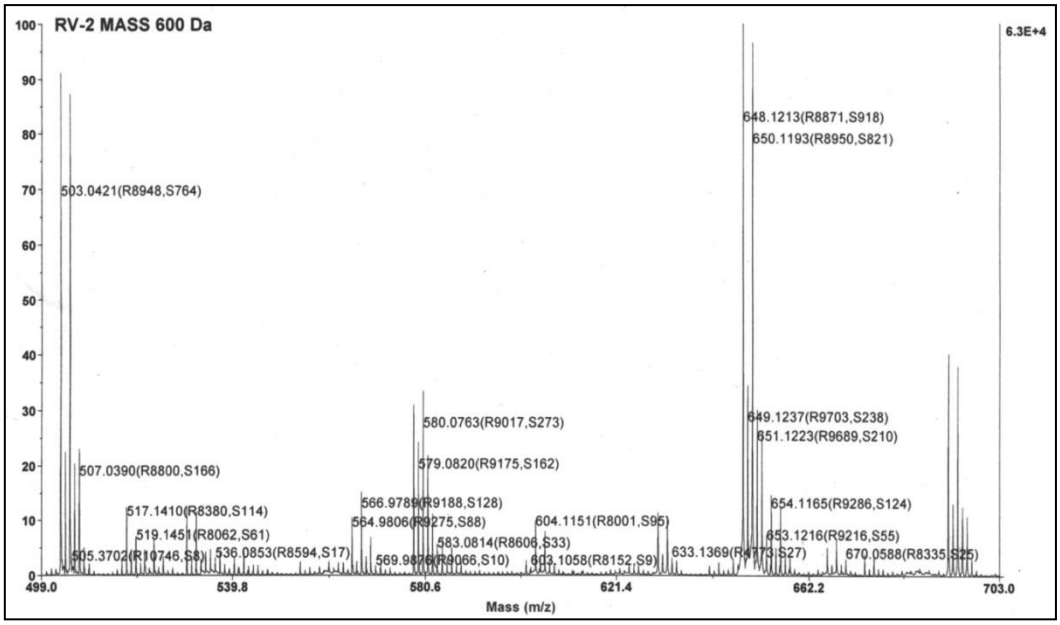

(f)

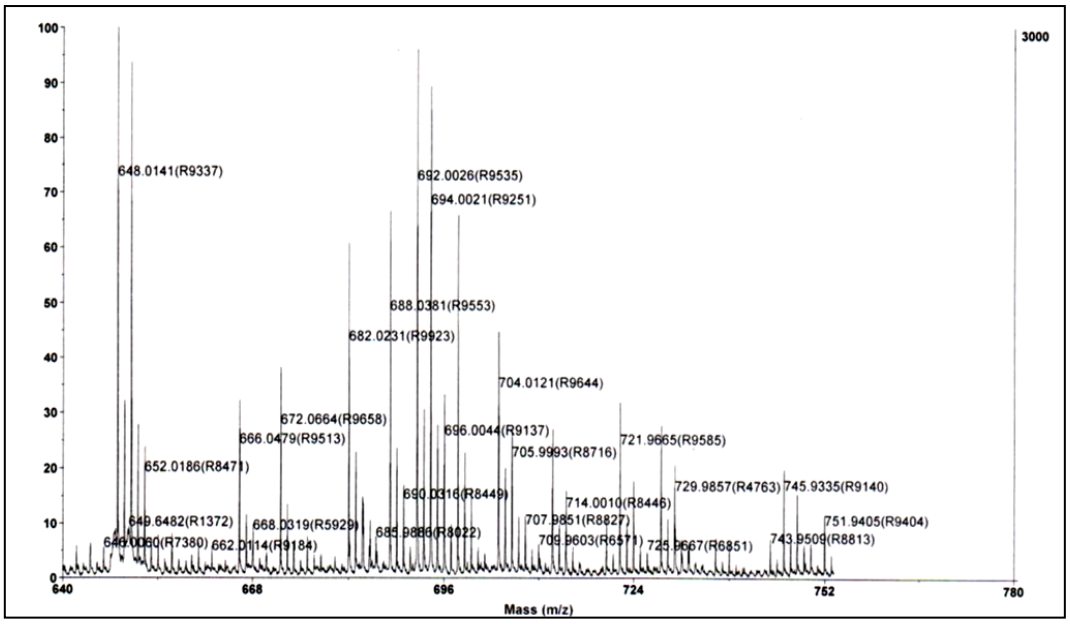

(g)

Fig. 10. MALDI-TOF MS spectra (a) for **1**, (b) for **2**, (c) for **3**, (d) for **5**, (e) for **6**, (f) for **7** and (g) for **8**

5.2.10. Thermogravimetric study

The thermogravimmetric analysis of $\mathbf{L^1}$-$\mathbf{L^2}$ and their transition metal complexes **1-8** were performed to investigate their thermal stability and thermal degradation patterns. The thermal analysis of individual samples was carried out in a temperature range from room temperature to 550 °C or 750 °C. The thermogravimetric plots for these compounds are shown in (Fig. 11). The heating rate was suitably controlled at 10º C

min^{-1} under nitrogen atmosphere. The differential weight losses over a range of temperature, rate of thermal decomposition and the residual masses corresponding to final degradation products are summarized in [Table 4]. The thermogravimetric plots (Fig. 11) of $\mathbf{L^1}$ and $\mathbf{L^2}$ clearly give a sharp endothermic peak on DTA curves at 187.5 and 220.3 ºC respectively, without any significant mass loss on DTG curves, due to the phase change that can be assigned to the melting points of these compounds. The TG curves further demonstrate that $\mathbf{L^1}$ and $\mathbf{L^2}$ decomposed completely with a maximum rate of decompositions (0.304 mg min^{-1} for L^1 and 0.172 mg min^{-1} for L^2) recorded at 301.4 and 345.5.3 °C respectively, on DTG curves. The stable residual mass of 14%, obtained for L^1 may corresponds to the char whereas 100% decomposition of L^2 was recorded on its TG curve (Fig. 11) up to 350 °C.

Thermograms of the complexes **1-8** clearly reveal that their decompositions start before their melting points and maximum decomposition is observed for copper(II) complex **8** with the maximum rate of decomposition of 0.466 mg min^{-1} at 368.1 °C. TG curves for 1-8 clearly suggests the thermal stability of these complexes up to 320 °C wherein complexes **4** and **5** displayed maximum stability and their degradation start after 400 °C. Notably, complex **7** exhibit quick mass loss on TG curve with a maximum rate of decomposition of 2.214 mg min^{-1} at 357.3 °C observed on its DTG curve.

Table 4 Thermal Decomposition of the κ^3-*N,O,O*-Schiff base metal complexes **1-8**

Entry	Steps	Temperature range(^{0}C)	Weight loss (%)	DTA Peak (°C)	DTG Peak (°C)	Rate of decomposition (mg min^{-1})
L^1	I	200-320	86	187.5, 194.9	301.4	0.304
L^2	I	210-350	100	220.3	345.5	0.172
1	I	340-750	49.47	404.8	405.5	1.345
2	I	380-750	51	418.8	418.8	1.061
3	I	360-750	41.34	400.2	399.3	0.284
4	I	400-750	43.5	425.9	426.6	1.116
5	I	420-750	52.8	450.4	451.2	1.139
6	I	380-750	49	410.6	411.3	0.956
7	I	320-750	59	359.3	357.3	2.214
8	I	310-750	61.5	363.9	368.1	0.466

In the case of compound **3** the thermal decomposition was observed in the range from 30-750 °C. There were two stages of decomposition one from 300-415 °C and other one 415-750 °C. In the both the stages 41.34% weight loss was observed. There was

no mass loss was observed from room temperature to 300 °C. In the case of stage first, the endothermic peak at 400.2 °C was observed on DTA curve, which is accompanied by weight loss confirming.

In the case of compound **6** the thermal decomposition were observed in two stages, one from 190-450 °C and other one 450-750 °C. In the both the stages 49% weight loss was observed. There was no mass loss was observed from room temperature to 190 °C. In the case of stage first, the endothermic peak at 410.6 °C was observed on DTA curve, which is accompanied by weight loss confirming (Table 4).

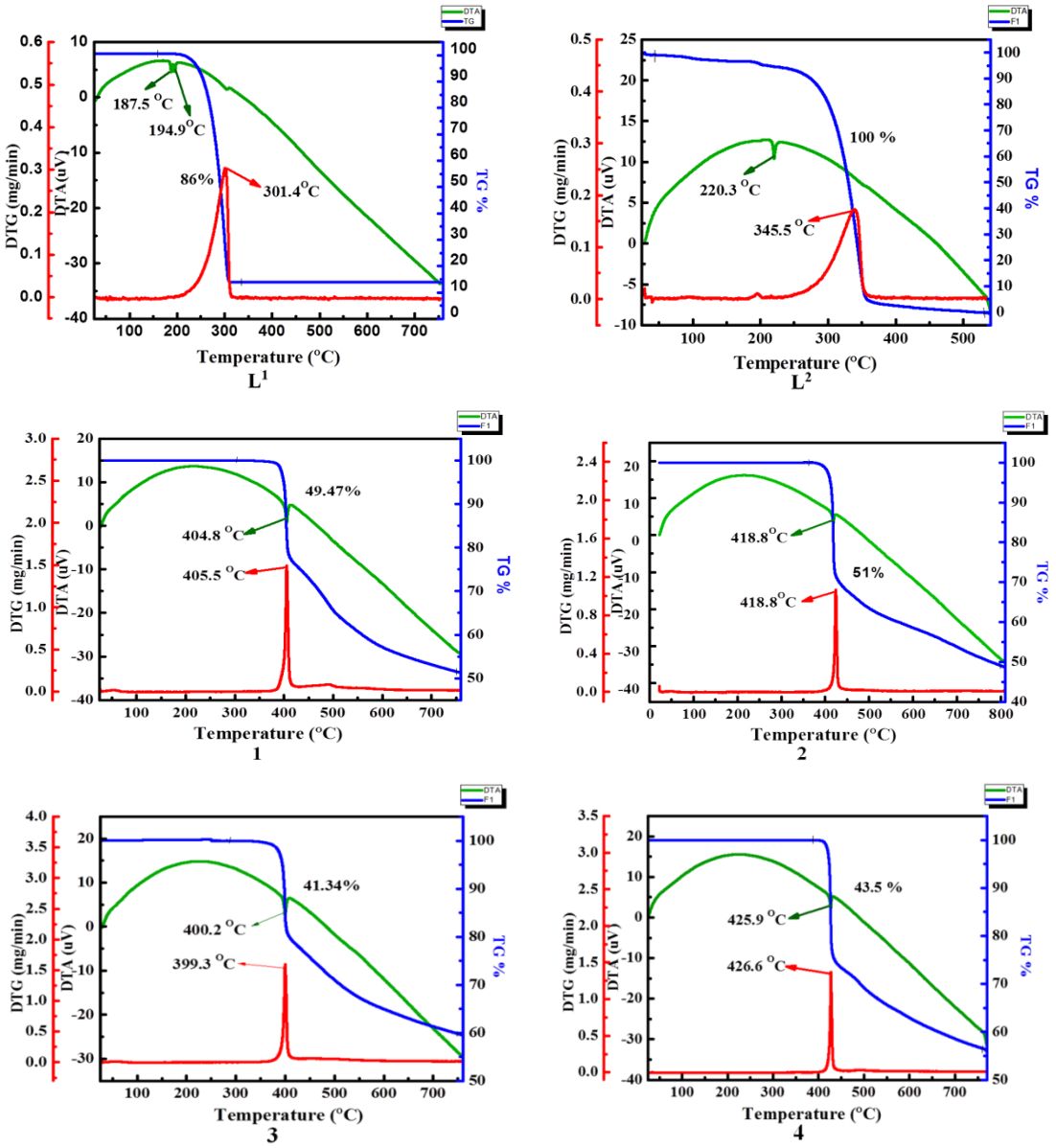

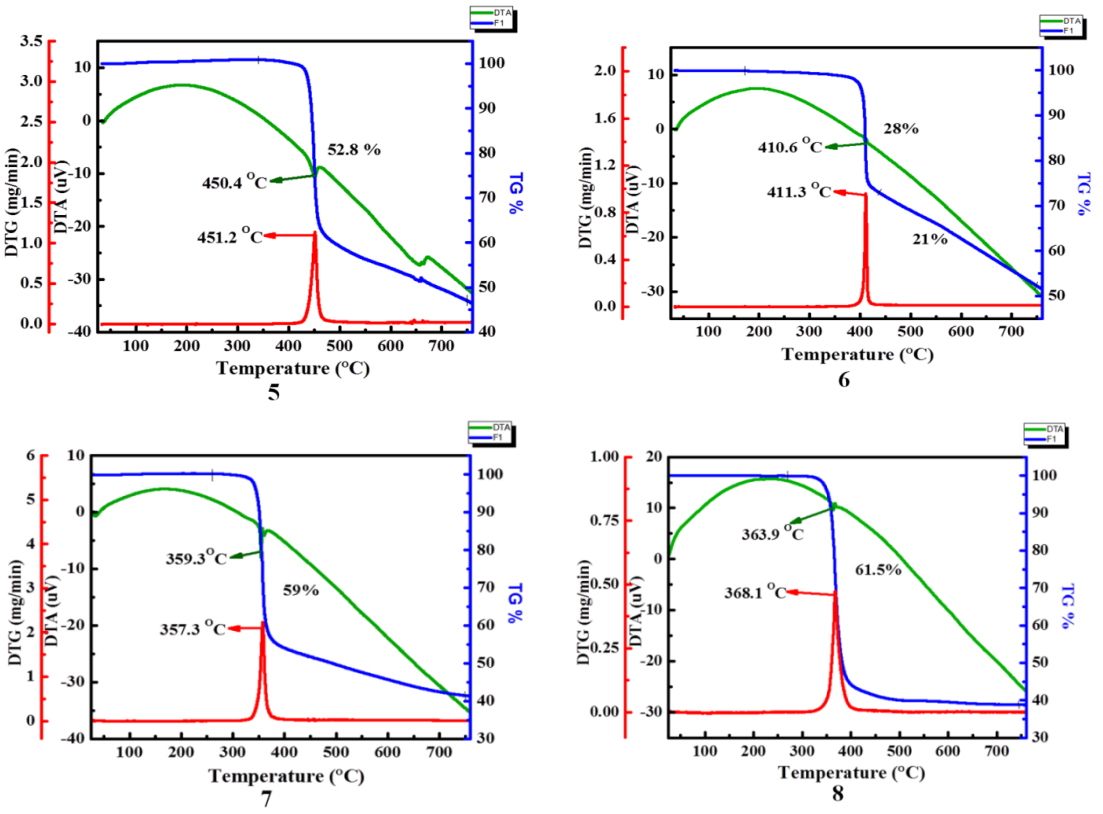

Fig. 11. TG/DTA spectra of the κ^3-*N*,*O*,*O*-Schiff base-L^1, κ^3-*N*,*O*,*O*-Schiff base-L^2 and metal complexes **1-8**.

5.2.11. Cyclic voltammetric study

The electrochemical behavior of 0.1 mM solutions of $\mathbf{L^1}$, $\mathbf{L^2}$ and transition metal complexes **1-3** and **6-8** have been investigated by cyclic voltammetric (CV) study in DMSO containing 0.1 M tetra-n-butylammonium bromide as the supporting electrolyte, at a platinum working electrode. The cyclic voltammogram for these are summarized in Fig. 12 and the results are given in Table 5. Electrochemical examination of $\mathbf{L^1}$ and $\mathbf{L^2}$, initially carried out which clearly demonstrates a quasi-reversible redox behavior and L^1 and irreversible electro oxidation of L^2. A quasi-reversible nature of both the redox couples of $\mathbf{L^1}$ is confirmed by the ratio of the current intensity of the cathodic and anodic peaks which are different from unity.

Compared to the cyclic voltammogram of $\mathbf{L^1}$ and $\mathbf{L^2}$, their complexes **1-3** and **6-8** did not display any additional peak, in the cathodic or anodic scan under the similar experimental conditions *i.e.* voltammograms of these exhibit similar feature, except the differences in the cathodic/anodic current peak heights (Fig. 12). This suggests that the complexes are primarily electro active with respect to the ligand fragment while the redox active transition metal cations are apparently present in silent mode.

The silent nature of transition metal ions in the presence of dominant electro-active ligands has previously been observed in a number of cases. [35-37] Further, electrochemically equivalence of multiple ligand units in these complexes is confirmed by emergence of single quasi-reversible or irreversible waves.

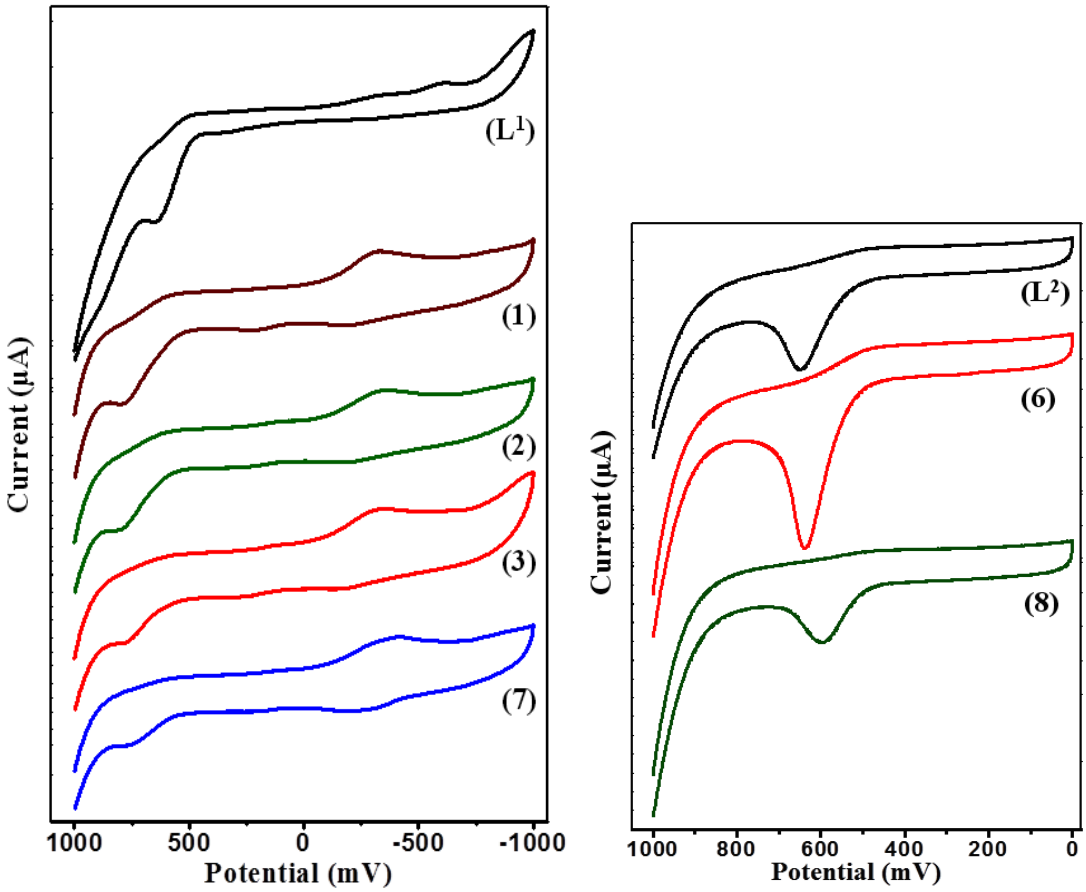

Fig. 12. Cyclic voltamograms L^1, L^2 and transition metal complexes **1-3** and **6-8**. Potential were measured vs. Ag/AgCl reference electrode at scan rate of 500 mV/s; supporting electrolyte: tetra-n-butylammonium bromide (0.1 M); complex concentration: 0.0001 M.

Table 5 Electrochemical data for the κ^3-*N*,*O*,*O*-Schiff base-L^1, κ^3-*N*,*O*,*O*-Schiff base-L^2 and metal complexes.

Entry	Ep_c(mV)	Ip_c(µA)	Ep_a(mV)	Ip_a(µA)	$E_{1/2}$(mV)	ΔEp(mV)
L^1	-635	2.391	-430	0.203	-322	205
L^2	-	0.860	649	11.624	555	-
1	-327	5.678	-199	0.524	-263	128
2	-365	5.266	-172	0.648	-268	193
3	-336	6.348	-147	1.019	-241	189
6	-	2.250	638	21.418	537	-
7	-419	4.989	-191	1.222	-305	228
8	-	0.273	597	6.731	528	-

5.3. Conclusion

A series of neutral mononuclear transition metal complexes [M^{II}-κ^3-bis-*N*,*O*,*O*-tridentate Schiff base-L^1/ L^2] {L^1; M^{II} = Co (**1**), Ni (**2**) or Zn (**3**); L^2; M^{II} = Co (**4**), Ni (**5**) or Zn (**6**)} and [M^{II}-κ^2-bis-*N*,*O*-bidentate Schiff base-L^1/ L^2] {L^1; M^{II} = Cu (7); L^2; M^{II} = Cu (8)} were synthesized from novel Schiff base lignads L^1-L^2 and characterized satisfactorily by using standard spectroscopic and thermogravimetric methods. The unambiguous crystal structure for $\mathbf{L^1}$, $\mathbf{L^2}$, complexes **2** and **3** were determined by means of single crystal X-ray diffraction technique. The spectral studies along with magnetic susceptibly measurements clearly suggest the κ^3-*N*,*O*,*O*-tridentate- coordination mode of L^1 and L^2 towards cobalt(II), nickel(II) and zinc(II) metal ions in **1-6** while κ^2-*N*,*O*-bidentate-coordination mode towards copper(II) metal ions in **7** and **8**. All the compounds feature a direct band gap semiconducting nature and exhibit band gap energy in the range of 1.7-2.23 eV. A majority of compounds fluoresces in the visible region when excited at lower wavelengths with significant bathochromic shifts. The cyclic voltamograms of these compounds revealed that the mononuclear complexes are primarily electro active with respect to the ligand fragment wherein the redox active transition metal cations are apparently present in silent mode.

5.4. Experimental Section

5.4.1. Materials and measurements

All solvents were purchased from the commercial sources and were freshly distilled prior to use. Reagents such as metal acetates $Co(OAc)_2.4H_2O$, $Ni(OAc)_2.4H_2O$, $Cu(OAc)_2.H_2O$ and $Zn(OAc)_2.2H_2O$ were purchased from Merck and these were used without further purification. ^1H and ^{13}C NMR spectra were recorded on a Bruker 400 MHz instrument. IR spectra (KBr pellets) were recorded on a Bruker instrument. UV-visible spectra (DMSO solution) were recorded on a Perkin Elmer Lambda 35 UV-visible spectrophotometer and the optical characterizations in solid state were performed by UV-visible transmittance measurements. Florescence was recorded on JASCO make spectrofluorimeter model FP-6300. Thermogravimetric analysis was performed on a SII TG/ DTA 6300 under flowing N_2 with a heating rate of 10 °C min^{-1}. Maldi TOF-MS were recorded from IIIM, CSIR Jammu and ESR analysis were done by E-112 ESR Spectrometer from SAIF IIT Bombay. Magnetic Moments were

done on Faraday Valance-2002 (1.0 Tesla), balance-Mettler UMx5, at room temperature. Electrochemical measurements were performed on a CH Instruments 600C potentiostat, using a Pt disk as the working electrode, Ag/AgCl as the reference electrode and a Pt wire as the counter electrode. Voltammograms were recorded by using anhydrous solutions of the metal complexes in dichloromethane (1.0 mM) containing tetra-n-butylammoniumhexafluoro phosphate (0.1M) as supporting electrolyte.

5.4.2. Synthesis of L^1 and L^2

3-aminocoumarin (1000 mg, 6.2 mmol,) was mixed with catalytic amount of glacial acetic acid in 20 ml toluene and solution was gently warm. To this solution, added equivalent amount of salicyladehyde (0.66 ml, 6.2 mmol) or *o*-hydroxy naphthaldehyde (1070 mg, 6.2 mmol) and the reaction mixture was refluxed for 4 hours using with dean stark apparatus. The reaction mixture was allowed to cool at room temperature. Solvent was removed in rotatory evaporator. The solid residue was washed with chilled ethanol followed by diethyl ether and vacuum dried to yield the Schiff base ligands 3-[(2-hydroxyphenylmethylidene amino) coumarin (HL^1) or 3-[(2-hydroxy-1-naphthylmethylidene amino)coumarin (HL^2).

HL^1. Orange solid. MW: 265.2. Yield: 1629 mg (98.9%). Anal. Calcd. for $C_{16}H_{11}NO_3$: C 72.45, H 4.15, N 5.28 %. Found: C 72.58, H 4.01, N 5.15 %. ^{1}H NMR ($CDCl_3$, 400 MHz): δ (ppm) 12.983 (s, 1H, O*H*); 9.486 (s, 1H, *H*C=N); 7.72 (s, 1H, *Ph*); 7.59-7.56 (d, 2H, *Ph*); 7.46 (m, 1H, *Ph*); 7.40-7.34 (m, 3H, *Ph*); 7.03 (m, 2H, *Ph*). ^{13}C NMR ($CDCl_3$, 400 MHz): δ (ppm) 167.14, 161.44, 157.92, 152.15, 149.04, 137.04, 134.31, 134.13, 133.38, 131.55, 128.12, 124.97, 119.42, 117.39, 116.46, 111.03. FTIR (cm^{-1}): 3424.12, 3046.70, 1721.48, 1491.15, 1114.80, 1058.74. GC-MS: m/z 265 [M^+].

HL^2: Reddish yellow solid. MW: 315.3. Yield: 1930 mg (98.6%). Anal. Calcd. for $C_{20}H_{13}NO_3$: C 76.18, H 4.16, N 4.44 %. Found: C 76.34, H 4.01, N 4.12 %. ^{1}H NMR ($CDCl_3$, 400 MHz): δ (ppm) 15.188 (s, 1H, O*H*); 10.196 (s, 1H, *H*C=N); 8.208 (d, 1H, *Ph*); 7.860 (d, 1H, *Ph*); 7.757-7.721 (t, 2H, *Ph*); 7.596-7.538 (m, 3H, *Ph*); 7.42-7.33 (m, 3H, *Ph*); 7.14 (d, 1H, *Ph*). ^{13}C NMR ($CDCl_3$, 400 MHz): δ(ppm) 167.77, 166.27, 159.37, 158.01, 156.27, 151.85, 136.98, 133.14, 131.26, 131.17, 130.70,

129.32, 128.36, 127.86, 125.02, 124.01, 121.05, 119.73, 116.51, 109.80. FTIR (cm^{-1}): 3410.49, 3031.23, 1716.04, 1463.67, 1170.01, 1077.02. GC-MS: m/z 315 [M^+].

5.4.3. Synthesis of mononuclear transition metal complexes 1-8

To a stirred solution of HL^1 (530.4 mg, 2.0 mmol) or HL^2 (630.6 mg, 2.0 mmol) in dry ethanol in two necked round bottom flask were added slight excess of sodium carbonate (233.2 mg, 2.2 mmol) and $Co(OAc)_2.4H_2O$ (249 mg, 1.0 mmol), $Ni(OAc)_2.4H_2O$ (248 mg, 1.0 mmol), $Cu(OAc)_2.H_2O$ (199 mg, 1.0 mmol) or $Zn(OAc)_2.2H_2O$ (218 mg, 1.0 mmol) under nitrogen atmosphere.

The reaction mixture was allowed to reflux for 4 hours and thereafter allowed to cool at room temperature. The precipitates obtained, were filtered off, washed with hot ethanol followed by distilled water, several times to ensure the removal of un-reacted ligands, metal acetates and sodium carbonate respectively. The solid residue was dried under high vacuum for 2-3 hours before taken for the analysis.

Complex 1: Brown solid. MW: 587.4. Yield: 487.5 mg (83.2%). Anal. Calcd. for $C_{32}H_{20}N_2O_6Co$: C 65.43, H 3.43, N 4.77%. Found: C 65.53, H 3.33, N 4.57%. FTIR (cm^{-1}): 3033.18, 1664.06, 1451.58, 1130.63, 1101.25. ESI-MS: m/z 588.06 $[M+H]^+$.

Complex 2: Dark brown solid. MW: 587.2. Yield: 563 mg (96.1%). Anal. Calcd. for $C_{32}H_{20}N_2O_6Ni$: C 65.45, H 3.43, N 4.77, Ni 10.0%. Found: C 64.98, H 3.48, N 4.61%. FTIR (cm^{-1}): 3037.31, 1660.27, 1435.19, 1134.13, 1104.40. ESI-MS: m/z 587.16 $[M]^+$.

Complex 3: Red solid. MW: 593.9. Yield: 520 mg (87.8%): Anal. Calcd. for $C_{32}H_{20}N_2O_6Zn$: C 64.72, H 3.39, N 4.72, Zn 11.01%. Found: C 65.12, H 3.29, N 4.82%. ^1H NMR (DMSO-d_6, 400 MHz): δ (ppm) 9.017 (s, 2H, *H*C=N); 8.484 (s, 2H, *Ph*); 7.809 (d, 2H, *Ph*); 7.685 (t, 2H, *Ph*); 7.487 (m, 6H, *Ph*); 7.259 (m, 2H, *Ph*); 6.543-6.46 (m, 4H, *Ph*). FTIR (cm^{-1}): 3036.70, 1689.26, 1436.02, 1132.15, 1098.96. ESI-MS: m/z 593.06 $[M]^+$.

Complex 4: Brown solid. MW: 687.5. Yield: 579.9 mg (84.1%): Anal. Calcd. for $C_{40}H_{24}N_2O_6Co$: C 69.87, H 3.52, N 4.07, Co 8.57%. Found: C 70.06, H 3.41, N 4.27%. FTIR (cm^{-1}): 3028.47, 1663.90, 1455.80, 1131.92, 1107.56. ESI-MS: m/z 688.02 $[M+H]^+$.

Complex 5: Dark brown solid. MW: 687.3. Yield: 610 mg (88.9%): Anal. Calcd. for $C_{32}H_{20}N_2O_6Ni$: C 69.90, H 3.52, N 4.08, Ni 8.54%. Found: C 70.01, H 3.49, N 4.02,

Ni 8.60%. FTIR (cm^{-1}): 3027.92, 1659.49, 1428.73, 1134.54, 1111.74. ESI-MS: m/z 687.10 $[M]^+$.

Complex 6: Red solid. MW: 694.0. Yield: 502 mg (72.6%): Anal. Calcd. for $C_{40}H_{24}N_2O_6Zn$: C 69.23, H 3.49, N 4.04, Zn 9.42%. Found: C 69.15, H 3.41, N 4.11, Zn 9.40%. ^1H NMR (DMSO-d_6, 400MHz): δ (ppm) 9.674 (s, 2H, *H*C=N); 8.574 (s, 2H, *Ph*); 8.427 (d, 2H, *Ph*); 7.864 (d, 2H, *Ph*); 7.779 (d, 2H, *Ph*); 7.705 (d, 2H, *Ph*); 7.687-7.417 (m, 8H, *Ph*); 7.30-7.263 (t, 2H, *Ph*); 6.703 (d, 2H, *Ph*).FTIR (cm^{-1}): 3033.65, 1677.97, 1460.09, 1134.06, 1102.60. ESI-MS: m/z 695.09 $[M+H]^+$.

Complex 7: Yellowish brown solid. MW: 592.0. Yield: 547 mg (92.6%): Anal. Calcd. for $C_{32}H_{20}N_2O_6Cu$: C 64.92, H 3.40, N 4.73, Cu 10.73%. Found: C 65.13, H 3.42, N 4.81, Cu 10.68%. FTIR (cm^{-1}): 3050.07, 1720.75, 1445.76, 1125.62, 1082.17. ESI-MS: m/z 687.10 $[M]^+$.

Complex 8: Dirty yellow solid. MW: 692.1. Yield: 5667 mg (96.5%): Anal. Calcd. for $C_{40}H_{24}N_2O_6Cu$: C 69.41, H 3.49, N 4.05, Cu 9.18%. Found: C 70.12, H 3.42, N 4.32, Cu 9.03%. FTIR (cm^{-1}): 3037.95, 1737.88, 1449.42, 1121.95, 1087.11. ESI-MS: m/z 692.0 $[M]^+$.

5.5. References

1. Maria, D. M. C.; da silva, R.; Jorge, M. G.; Ana,L. R. S.; Paula,C. F. C.; Schroder, B.; Manual, A. V. *J. Mol. Catal. A: Chem.* **2004**, *224*, 207.
2. Jarrahpour, A.; Khalili, D.; Clercq, E. D.; Salmi C.; Brunel J. M. *Molecules* **2007**, *12*, 1720.
3. Spinu, C.; Kriza, A. *Acta Chem. Slov.* **2000**, *47*, 179.
4. Morris, G. A.; Zhou, H.; Stern, C. L.; Nguyen, S. T. *Inorg. Chem.*, **2001**, *40*, 3222.
5. Chaudhuri, P.; Stockheim, C.; Wieghardt, K.; Deck, W.; Gregorzik, R.; Vahrenkamp, H.; Nuber, B.; Weiss, *J. Inorg. Chem*., **1992**, *31*, 1451, and references therein.
6. Uhlenbrock, S.; Krebs, B. *Angew. Chem., Int. Ed. Engl.*, **1992**, *31*, 1647;.
7. Murthy, N. N.; Karlin, K. D. *J. Chem. Soc., Chem.Commun*., **1993**, 1236.
8. Chen, X. -M.; Tong, Y. -X.; Mak, T. C. W. *Inorg. Chem*., **1994**, *33*, 4586.
9. Bazzicalupi, C.; Bencini, A.; Bianchi, A.; Fusi, V.; Paoletti, P.; Valtancoli, B. *J. Chem. Soc., Chem. Commun.*, **1994**, 881.
10. Bazzicalupi, C.; Bencini, A.; Bianchi, A.; Fusi, V.; Mazzanti, L.; Paoletti, P.; Valtancoli, B. *Inorg. Chem.*, **1995**, *34*, 3003.
11. Bazzicalupi, C.; Bencini, A.; Bianchi, A.; Fusi, V.; Paoletti, P.; Piccardi, G.; Valtancoli, B. *Inorg. Chem*., **1995**, *34*, 5622.
12. Yun, J. W.; Tanase, T.; Lippard, S. J. *Inorg. Chem*., **1996**, *35*, 7590.
13. Yamami, M.; Tanaka, M.; Sakiyama, H.; Koga, T.; Kobayashi, K.; Miyasaka, H.; Ohba, M.; Okawa, H. *J. Chem. Soc., Dalton Trans*., **1997**, 4595.
14. Meyer, F.; Rutsch, P. *Chem. Commun*., **1998**, 1037.
15. Yu, T.; Zhang, K.; Zhao, Y.; Yang, C.; Zhang, H.; Qian, L.; Fan, D.; Dong, W.; Chen, L.; Qiu, Y. *Inorg. Chim. Acta*, **2008**, *361*, 233.
16. Al-Shiri, A. S. *Spectrochim. Acta (A)* **2004**, *60*, 118.
17. Bolos, C. A.; Papazisis, K. T.; Kortsaris, A. H.; Voyatzi, S.; Zambouli, D.; Kyriakidis, D. A. *J. Inorg. Biochem*. **2002**, *88*, 25.
18. Bolos, C. A.; Nikolov, G. St.; Ekateriniadou, L.; Kortsaris, A.; Kyrikidis, D. A. *Metal-Based* Drugs, **1998**, *5*, 323.
19. Kadu, R.; Singh, V. K.; Verma, S. K.; Raghavaiah, P.; Shaikh, M. M. *J. Mol. Struct*. **2013**, *1033*, 298.

20. Raman, N.; Sobha, S.; Thamaraichelvan, A. *Spectrochimica Acta Part A* **2011**, *78*, 888.
21. Reddy, G. R.; Balasubramanian, S.; Chennakesavulu, K. *J. Mater. Chem. A* **2014**.
22. Wehrmann, P.; Mecking, S. *Organometallics*, **2008**, *27*, 1399.
23. Epstein, D. M.; Choudhary, S.; Churchill, M. R.; Keil, K. M.; Eliseev, A. V.; Morrow, J. R. *Inorg. Chem.* **2001**, *40*, 1591.
24. Orio, M.; Philouze, C.; Jarjayes, O.; Neese, F.; Thomas, F. *Inorg. Chem.* **2010**, 49, 646.
25. Verma, S. K.; Singh, V. K. *Polyhedron*, **2014**, *76*, 1.
26. (a) Lever, A.B.P. Inorganic Electronic Spectroscopy, Elsevier, Amsterdam, 1968. (b) Sacconi, L.; Ciampolini, M. *J. Chem. Soc.* **1964**, 276.
27. Lever A.B.P. *J. Chem. Edu*., **1968**, *45*, 711.
28. Ramam; N.; Kulandaisami, A.; Shunmugasundaram, A. *Trans Met Chem*., **2001**, *26*, 131.
29. (a) Mizobe, Y.; Hinoue, T.; Yamamoto, A.; Hisaki, I.; Miyata, M.; Hasegawa, Y.; Tohnai, N. *Chem. Eur. J*. **2009**, *15*, 8175; (b) Lee, K. -H.; Choi, C. -S.; Jeon, K. -S. *J. Photosci*. **2002**, *9*, 71; (c) Martens, S. C.; Zschieschang, U.; Wadepohl, H.; Klauk, H.; Gade, L. H. *Chem. Eur. J*. **2012**, *18*, 3498; (d) Valdés, A. C.; Pina-Luis, G.;. Rivero, I. A *J. Mex. Chem. Soc*. **2007**, *51*, 87; (e) Madrigal, D.; Pina-Luis, G.; Rivero, I. A. *J. Mex. Chem. Soc*. **2006**, *50*, 175.
30. Rapheal, P. F.; Manoj, E.; Kurup, M. R. P. *Polyhedron* **2007**, *26*, 818.
31. Davis, E. A.; Mott, N. F. *Philos. Mag*. **1970**, *22*, 903.
32. Habibi, M. H.; Talebian, N. *Acta Chim. Slov*. **2005**, *52*, 53.
33. Tauc. *J. Mater. Res. Bull*. **1970**, *5*, 721.
34. Petkovi, M.; Petrovi, B.; Savi, J.; Bugar, Z. D.; Markovi, J. D.; Momi, T.; Vasi, V. *Int. J.l of Mass Spectrom.* **2010**, *290*, 39.
35. (a) Singh, N.; Kumar, A.; Prasad, R.; Molloy, K. C.; Mahon, M. F. *Dalton Trans*. **2010**, *39*, 2667; (b) Singh, V.; Chauhan, R.; Gupta, A. N.; Kumar, V.; Drew, M. G. B.; Bahadur L.; Singh, N. *Dalton Trans*. **2014**, *43*, 4752.
36. Verma, S. K.; Singh, V. K. *J. Coord. Chem.* **2015**, 68, 1072-1087.
37. Kumar, A.; Chauhan, R.; Molloy, K. C.; Kociok-Kçhn, G.; Bahadur, L.; Singh, N. *Chem. Eur. J.* **2010**, *16*, 4307.

5.6. Spectra

5.6.1. NMR spectra

The NMR spectra of κ^3-*N*,*O*,*O*-Schiff base-L^1, 3 κ^3-*N*,*O*,*O*-Schiff base-L^2 and its diamagnetic metal complexes are summarized below as Figure S1 to S7.

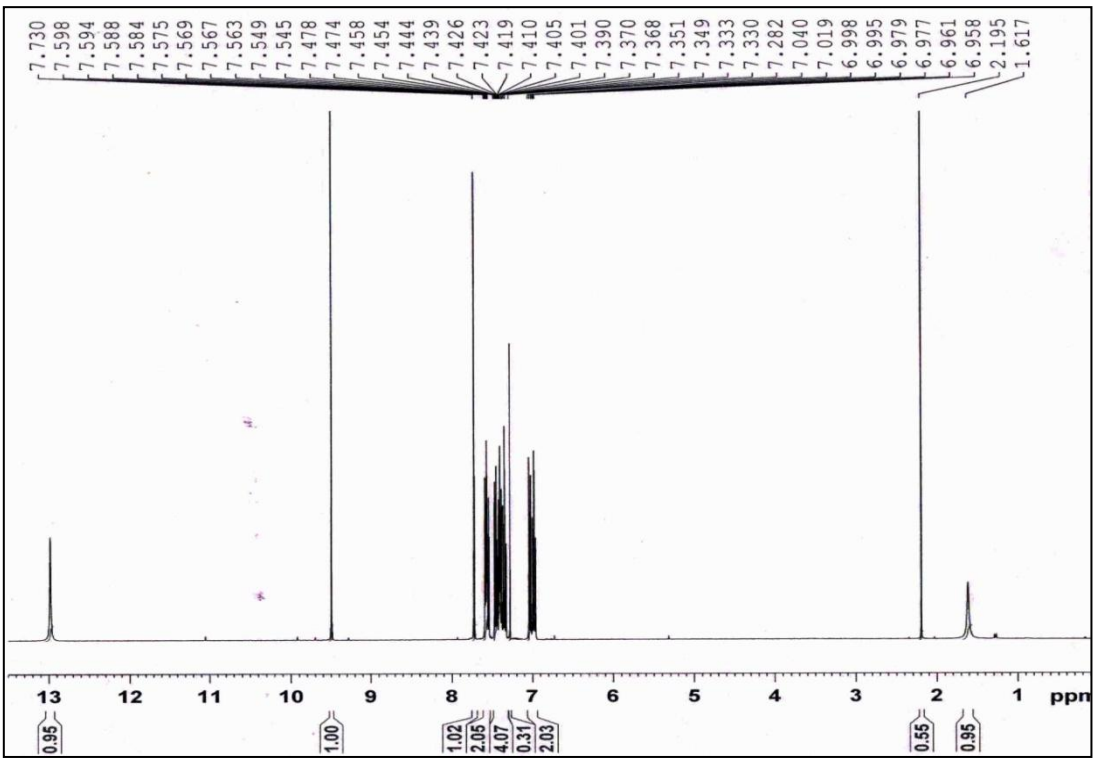

Figure S1. ^{1}H NMR spectrum of κ^3-*N*,*O*,*O*-Schiff base-L^1

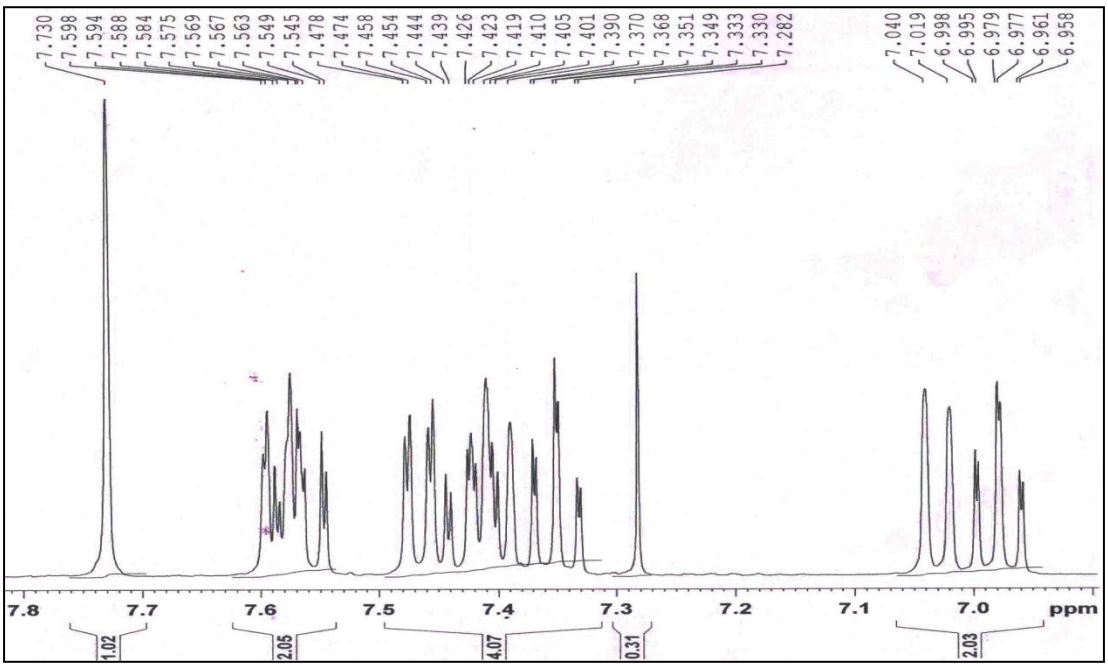

Figure S2. ^{1}H NMR spectrum of κ^3-*N*,*O*,*O*-Schiff base-L^1 Expended

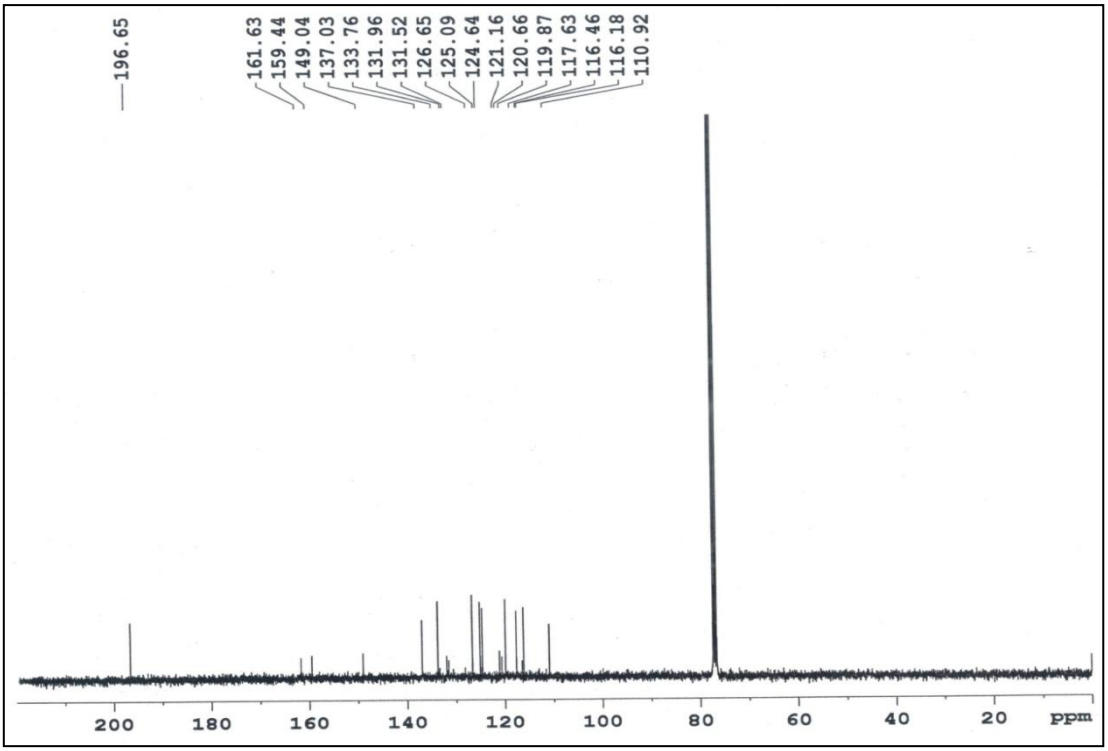

Figure S3. ^{13}C NMR spectrum of κ^3-*N*,*O*,*O*-Schiff base-L^1

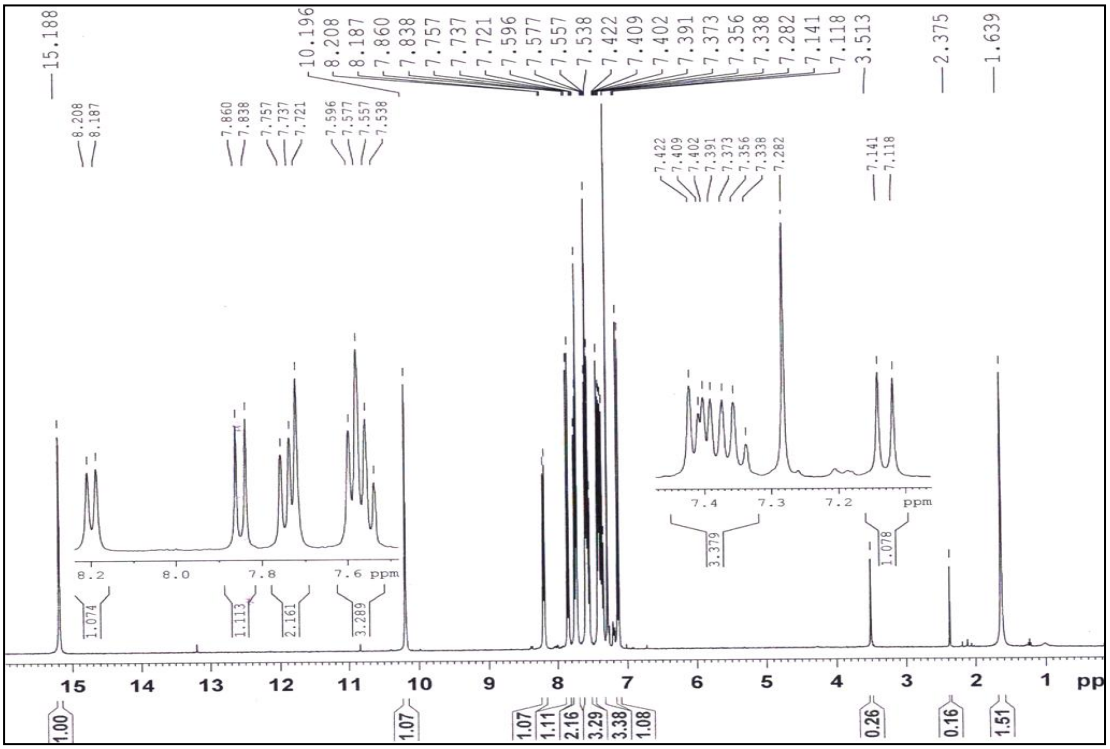

Figure S4. ^{1}H NMR spectrum of κ^3-*N*,*O*,*O*-Schiff base-L^2

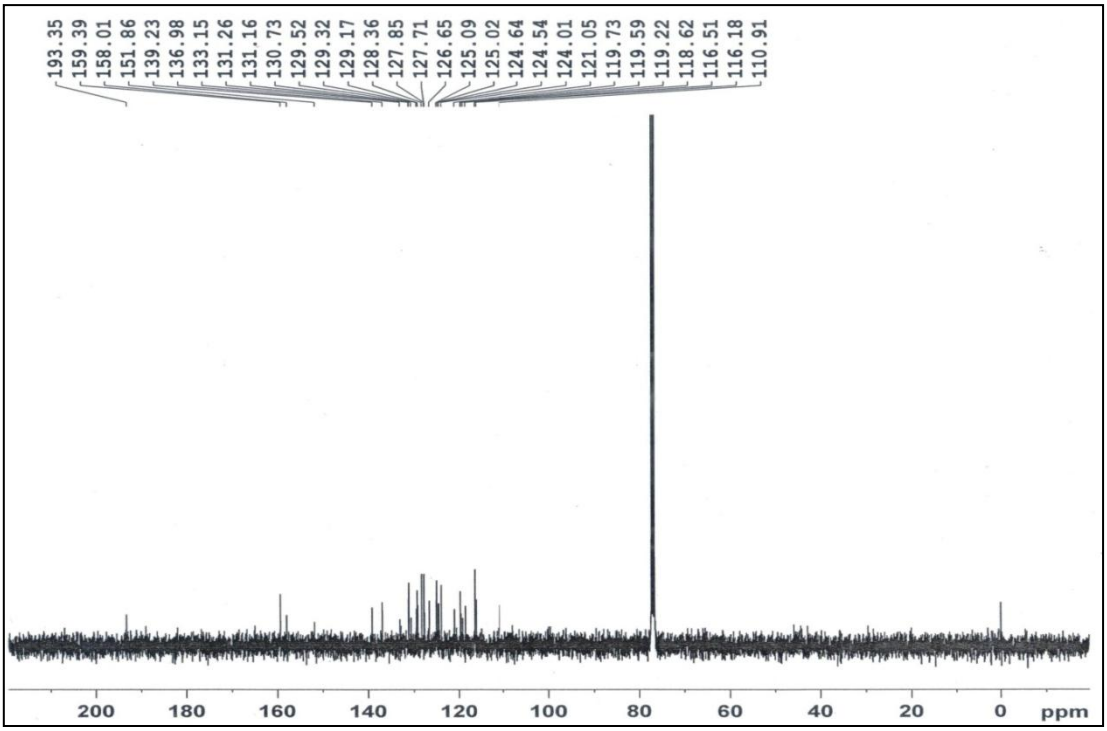

Figure S5. ^{13}C NMR spectrum of κ^3-*N,O,O*-Schiff base-L^2

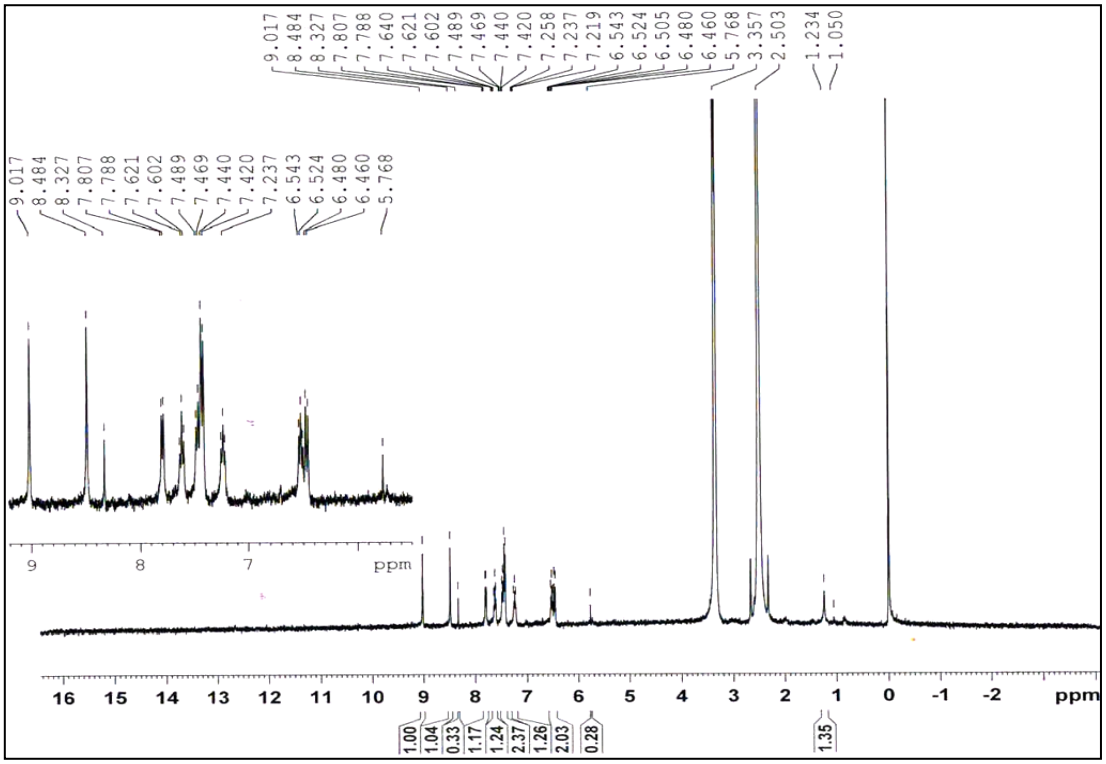

Figure S6. ^{1}H NMR spectrum of κ^3-*N,O,O*-Schiff base metal complex **3**.

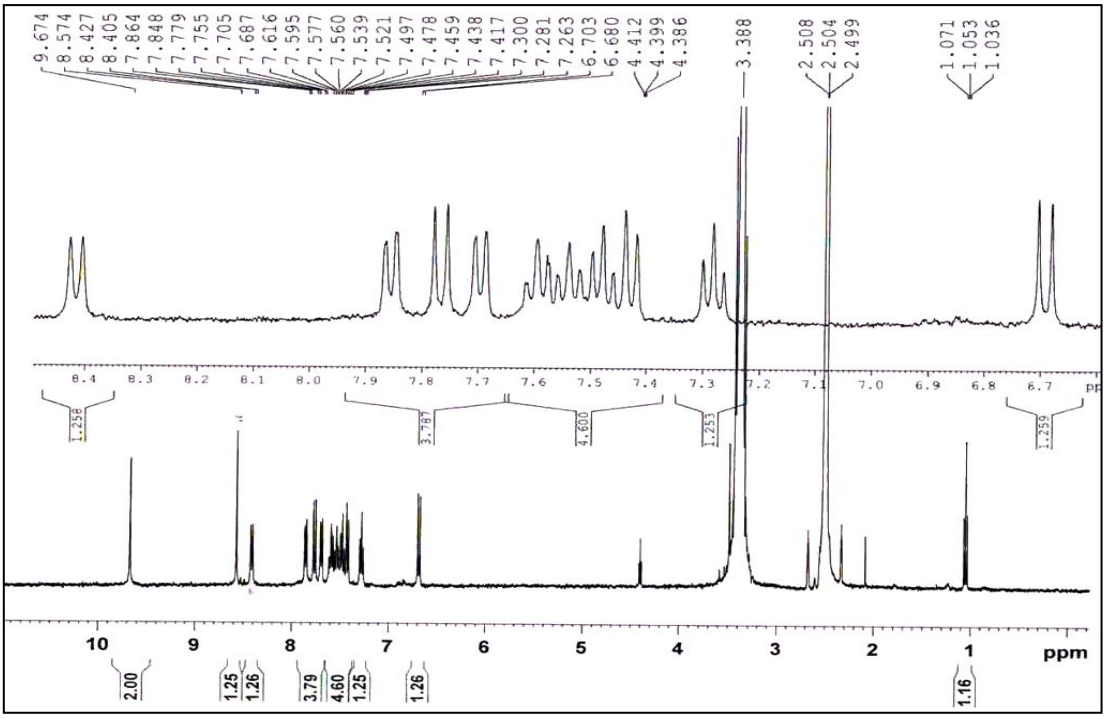

Figure S7. ^{1}H NMR spectrum of κ^{3}-*N*,*O*,*O*-Schiff base metal complex **6**.